Methods and Limitations of Line Source Simulation*

STEFAN FEISTEL,[1] *AES Member,* **AMBROSE THOMPSON,**[2] **AND**
(sfeistel@afmg.eu) (ambrose@martin-audio.com)

WOLFGANG AHNERT,[1] *AES Fellow*
(wahnert@afmg.eu)

[1]*Ahnert Feistel Media Group, 13189 Berlin, Germany*
[2]*Martin Audio, High Wycombe, Bucks, HP12 3SL, UK*

Although line array systems are in widespread use today, investigations of the requirements and methods for accurate modeling of line sources are scarce. In previous publications the concept of the generic loudspeaker library (GLL) was introduced. It is shown that on the basis of directional elementary sources with complex directivity data finite line sources can be simulated in a simple, general, and precise manner. Measurement requirements are derived, and the limitations of this model are discussed. In addition, a second step of refinement is presented, namely, the use of different directivity data for cabinets of identical type based on their positions in the array. All models are validated by measurements. The approach presented is compared with other proposed solutions.

0 INTRODUCTION

With the advent of modern line arrays, sound reinforcement systems reached a new level of flexibility and performance, but also of complexity. Mechanical and DSP-based control capabilities opened the door, for example, to more effective solutions for speech transmission in reverberant spaces and to rapid deployment with higher reproduction quality in outdoor applications. But these advantages came at the cost of higher complexity in the configuration and use of the systems. As a result, simulation and measurement tools have become a necessity when designing and verifying such complex loudspeaker systems.

But modeling a line array is not trivial because it cannot be considered as a point source like a conventional loudspeaker. A line array represents a linearly extended sound source of finite size that is typically used into its near field. Due to the size, directivity, and weight of a complete line array, acquiring measurement data for the system as a whole is impractical as well.

Therefore new measurement and modeling methods must be developed. Besides the very basic approach of reducing a full line array to a point source, the Huygens composition is also practiced. Essentially one tries to measure and model the wavefront for each type of cabinet using many elementary point sources [1]–[3]. This model can describe both the near field and the far field of the loudspeaker, but usually it lacks generality in several aspects, as will be shown. Related more advanced techniques based on Rayleigh integrals over imagined planar surfaces in front of a cabinet have been implemented [4]–[6], but they still suffer from similar shortcomings.

We present a practical method of line array modeling. Based on the concepts of the generic loudspeaker library (GLL) [7], a description language for loudspeaker performance, and DISPLAY 1.6 software [8], [9], our approach uses directional point sources with complex directivity data (CDPS model). We show that by representing each type of cabinet by a full-sphere balloon measurement with magnitude and phase data the radiation behavior of the line array can be modeled easily and directly.

This concept is presented in two steps. First we derive mathematically how a line source of finite size can be decomposed into a set of smaller line sources, where each subsource can be measured and applied in its far field. We emphasize that the use of both magnitude and

*Presented at the 125th Convention of the Audio Engineering Society, San Francisco, CA, 2008 October 2–5; revised 2009 May 19.

phase data is crucial to predict the near- and far-field behavior of the system as a whole. In addition, simulations in MATLAB [10], EASE SpeakerLab [11], and the MATLAB-based calculation engine of DISPLAY 2.0 [12] demonstrate the practical feasibility of the approach and its limitations.

In a second step the data for several real-world line array systems are used to compare prediction results with measurements. Here we also introduce another important finding, which allows us to increase simulation accuracy with a simple modification. We show that the measurement data for the outer cabinets at the top and bottom of the array can deviate significantly from those for the inner cabinets. This is mainly due to the varying acoustic support offered by neighboring cabinets and shadowing effects. Some improvement can already be accomplished when during the data acquisition the loudspeaker cabinet is measured with one top and one bottom neighbor in place. This is underlined by a comparison between prediction and measurement results. But considering the position of individual cabinets within the line array can further improve the match between simulation and measurement, as we will demonstrate in a detailed comparison of this refined approach with the measurement results for the entire system and the results of the simple calculation approach using identical cabinets. As a conclusion we make some comparisons with alternative methods, such as the Huygens approach.

To summarize, Section 1 gives a general overview of the concept of line sources and how they can be modeled. Section 2 reviews the GLL concept and introduces the CDPS method to predict the sound field radiated by a line array. We demonstrate the practical accuracy of this approach in Section 3 and discuss alternative models in Section 4.

1 LINE SOURCES

In this section we review the concept of the sound-radiating line source and its practical realization as a line array.

1.1 General Description

In a simple formulation the complex sound pressure $\tilde{p}$ created by an ideal line source of finite size L at a given receiver location in polar coordinates (r, θ, φ) can be described by

$$\tilde{p}(r,\theta,t) = \tilde{A}_0 \int_{-L/2}^{L/2} \frac{1}{r'} e^{j(\omega t - kr')}\, dx \tag{1}$$

where $r' \equiv r'(x)$ is the distance between a point on the line source and the receiver while we integrate over the length of the line in increments dx (see Fig. 1). Furthermore ω is the radial frequency, k the wavenumber, t the time, and $\tilde{A}_0$ the complex amplitude of the source [13]. Due to the symmetry of the arrangement the relationship is independent of the angle φ.

This integral cannot be solved directly. Analytical solutions are possible for asymptotic cases, such as under far-field condition. In any other case the integral has to be evaluated numerically.

1.2 Far-Field Approximation

In the far field of the source one can assume that the distance between receiver and source location is much greater than any characteristic dimension of the source. Assuming $r \gg L$, one can substitute r' by r in the denominator of the integrand in Eq. (1). The phase term in the exponent requires more care. Its first-order approximation for large r is $r' = r - x \sin\theta$. We obtain

$$\tilde{p}(r,\theta,t) = \frac{\tilde{A}_0}{r} e^{j(\omega t - kr)} \int_{-L/2}^{L/2} e^{jkx\sin\theta}\, dx. \tag{2}$$

One can see here already that the result will be a spherical wavefront, represented by the first factor, which is weighted by an angle- and frequency-dependent complex correction, represented by the second factor. The solution for the integral is

$$\tilde{p}(r,\theta,t) = \frac{\tilde{A}_0 L}{r} \left[\frac{\sin\left(\frac{1}{2}kL\sin\theta\right)}{\frac{1}{2}kL\sin\theta} \right] e^{j(\omega t - kr)}. \tag{3}$$

As a result the time-independent acoustic pressure amplitude $P = |\tilde{p}|$ for the far field can be written as

$$P(r,\theta) = P_{\text{axial}}(r)\Gamma(\theta) \tag{4}$$

where

$$\Gamma(\theta) = \left| \frac{\sin\left(\frac{1}{2}kL\sin\theta\right)}{\frac{1}{2}kL\sin\theta} \right| \tag{5}$$

is the directional factor as a function of the angle θ and

$$P_{\text{axial}}(r) = \frac{|\tilde{A}_0|L}{r} \tag{6}$$

is the amplitude of the on-axis far-field pressure amplitude as a function of the distance r. It is obvious that in the far field the axial pressure is proportional to $1/r$. This means that the line source can be approximated by a point source when considering locations in the far field.

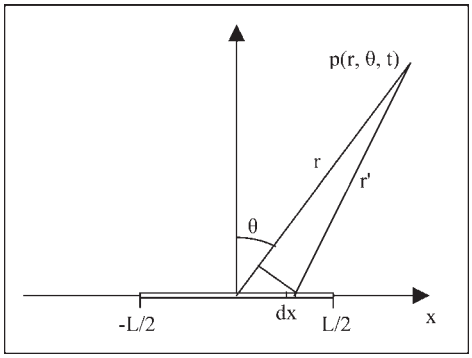

Fig. 1. Geometry of Eq. (1).

1.3 Numerical Solution

In the near field of the source, where r is of the same order of magnitude as L, Eq. (1) can only be solved numerically. For this purpose the integral is discretized and transformed into a sum,

$$\tilde{p}(r,\theta,t) = \tilde{A}_0 \frac{L}{N} \sum_{i=1}^{N} \frac{1}{r_i'} e^{j(\omega t - k r_i')}. \quad (7)$$

The accuracy of this approach is governed by the resolution L/N. It is commonly accepted that for a given upper frequency limit or wavelength, the resolution should be $L/N \leqslant \lambda/2$.

1.4 Modeling Line Arrays

So far we have discussed the fundamentals of ideal finite line sources. In reality the approximation of an ideal line source, the so-called line array, finds widespread use. Several loudspeaker cabinets are combined to form a linear or even curved array of sources. Individual cabinets may reproduce the behavior of an ideal line source depending on the design, the frequency range considered, and the intended use.

For an array the overall sound pressure at the receiving location is typically the sum of the sound pressure functions of the individual elements k of the array,

$$\tilde{p}_{\text{sum}}(r,\theta,t) = \sum_{k=1}^{M} \tilde{p}_k(r,\theta,t) \quad (8)$$

where each contribution $\tilde{p}_k$ represents a particular cabinet in the line array of M elements.

Modeling a single line source or a combination of line sources as given by Eq. (1) is not simple. We can distinguish between three fundamentally different approaches used for the prediction of the radiated sound field.

- The point-source approach according to Eqs. (3)–(6) in several variations, which is always based on a far-field approximation on a certain level. The complex-directivity point-source (CDPS) model, which we describe in the next section, is an advanced derivation of this.
- The so-called Huygens method, which essentially uses Eq. (7) to reproduce the sound field of the array. More precisely, one considers the individual contributions to the sum as omnidirectional point sources that form a coherent wavefront [1]–[3].
- The so-called Rayleigh integral method, which is based on the Kirchhoff–Helmholtz equation. In general, at any given location the field radiated by a source is characterized by the integral of the sound potential over a closed surface around the source [4]–[6].

2 COMPLEX-DIRECTIVITY POINT-SOURCE MODEL

This part introduces the concept of the complex-directivity point source (CDPS). We derive the theoretical background of this model for the case of line arrays and demonstrate its accuracy by means of comparisons between sound-field measurements and predictions.

2.1 Overview

2.1.1 Point-Source Models

The description of sound sources by means of a point-source model has a long history. The following equation governs the propagation of a spherical wavefront as generated by a point source [13]:

$$\tilde{p}(\boldsymbol{r},f) = \frac{\tilde{A}(\varphi,\theta,f)}{|\boldsymbol{r}|} e^{-j\boldsymbol{k}\boldsymbol{r}}. \quad (9)$$

Here $\tilde{p}$ is the sound pressure at the receiver location $\boldsymbol{r}$ and as a function of frequency f. $\tilde{A}$ is the complex radiation function depending on angles $\varphi = \varphi(\boldsymbol{r})$ and $\theta = \theta(\boldsymbol{r})$. The distance dependence of the pressure function is expressed by the denominator as well as by the phase term $\boldsymbol{kr}$, where $\boldsymbol{k}$ is the wave vector.

In the computer model the spectral and directional properties of the point source are usually represented in a discrete form regarding frequency and angle. Discretizing Eq. (9) yields

$$\tilde{p}(\boldsymbol{r},f) = \frac{g[\hat{A}(\varphi_k,\theta_l,f_m),\boldsymbol{r},f]}{|\boldsymbol{r}|} e^{-j\boldsymbol{k}\boldsymbol{r}} \quad (10)$$

where $\hat{A}$ is now a complex-valued matrix $\hat{\boldsymbol{A}}_{k,l,m}$ based on discrete angles φ_k and θ_l and frequencies f_m. The interpolation function g provides a smooth transition between the given data points for intermediate locations.

From this it becomes clear that on the one hand the interpolation function has to be chosen carefully in order to provide smooth results and on the other hand the data contained in $\hat{A}$ have to fulfill certain requirements in order to allow for interpolation by g afterward. In particular the sampled data have to include all the information required for the subsequent modeling process. In practice this information, so-called polar data, is gathered typically either by measurement or by a computer model of the sound source.

When interaction between sources such as in Eq. (8) does not have to be modeled and phase information is of no relevance, magnitude-only data $\hat{A} = |\hat{A}|$ and $g = |g|$ will suffice since considerations are restricted to the modulus of $\tilde{p}$.

Based on that, some approaches utilize only the run time phase component $\boldsymbol{kr}$ in order to simulate source interaction based on magnitude-only directivity data. This assumes that the inherent phase response of the source is negligible and that the source data do not include any additional phase due to propagation delay, that is, $\arg \tilde{A} \approx 0$. In practice this assumption is often not correct and cannot be applied to cases such as Eq. (3), where the inherent phase response of the source cannot be neglected but is crucial to model combinations of multiple sources.

In consequence the CDPS model is used to describe the properties of a sound source in its entirety, that is, also with respect to phase. Here no assumptions are made regarding the phase component of $\hat{A}$, but it is assumed that the phase information can be provided by measurement (or a radiation model of the loudspeaker cabinet) at sufficient accuracy.

As will be shown in the following sections the CDPS model provides a straightforward and fast means to simulate the radiation characteristics of line arrays. This application is governed by the combination of Eq. (8) and (10) and can be expressed generally by

$$\tilde{p}_{\mathrm{sum}}(\boldsymbol{r}, f) = \sum_{n=1}^{M} \frac{g(\hat{A}_n)}{|\boldsymbol{r} - \boldsymbol{r}_n|} \mathrm{e}^{-\mathrm{j}\boldsymbol{k}_n (\boldsymbol{r} - \boldsymbol{r}_n)} \tag{11}$$

where $\boldsymbol{r}_n$ is the location of the point source representing a particular element n and $\hat{A}_n$ is the complex radiation function in matrix form for the far field of that element.

2.1.2 Generic Loudspeaker Library (GLL)

In previous publications [9], [14], [15] the authors showed the relevance of complex data, that is, magnitude and phase data, for the prediction of the sound field of interacting sources. At the same time conditions for the representative data $\hat{A}$ were derived, in particular regarding the frequency resolution, the angular resolution, and the measurement (sampling) distance in order to be able to interpolate phase data in a meaningful way [7], [14]. A new framework, the so-called generic loudspeaker library, was presented as well in order to describe sound sources in this manner formally [16]. Others have also demonstrated the increased accuracy of using complex data in simple DPS (directional point source) models together with interpolation methods [17] and investigated the spatial/frequency resolution requirement [18], [19]. We believe that this is the first time all these issues have been addressed together in a clear manner.

The GLL basically serves as a format or, more precisely, as a language to describe sound sources and combinations of sources, such as multiway loudspeakers, column loudspeakers, or arrays of loudspeakers. It allows to include complex directivity data for each source in adequate angular and spectral resolutions. The loudspeaker cabinet as a whole or individual transducers can be modeled as point sources. As a result this approach offers a new degree of freedom, namely, the possibility to model electronic configurability, such as with respect to equalization and crossover filters, as well as mechanical configurability, such as regarding the actual physical arrangement of multiple cabinets in a linear or curved array [20].

With the GLL implementation of the CDPS model in the acoustic simulation software EASE [21] the CDPS method has found, for the first time, widespread propagation beyond manufacturers' and universities' own software tools.

2.2 Application to Line Sources

It is quite obvious that if a loudspeaker can be approximated by a point source according to Eqs. (9) and (10), an array of such loudspeakers will—following the fundamentals of linear superposition—show the radiation behavior as described by Eq. (11), assuming we can incorporate the effects of neighboring sources on each other.

In practice many arrays of loudspeakers are claimed to be close to the mathematically ideal line source, which means that over the usable frequency range of the device the array acts approximately like a single line source. The usefulness of this attribute for curved arrays is beyond the scope of this paper. We will now show that any real-world line source can be described by the CDPS model.

2.2.1 CDPS Decomposition

Eq. (1) can be rewritten identically to a sum of partial integrals, each representing, for example, a cabinet of the line array,

$$\tilde{p}(r, \theta, t) = \tilde{A}_0 \sum_{n=1}^{M} \int_{-L/2+(n-1)L/M}^{-L/2+nL/M} \frac{1}{r'} \mathrm{e}^{\mathrm{j}(\omega t - kr')} \, \mathrm{d}x. \tag{12}$$

As a second step we can apply a coordinate transformation that places the origin central to the boundaries of each partial integral, $x_n = x - [-L/2 + (n-1/2)L/M]$. The corresponding transformations are applied to $r(x)$, $\theta(x)$, and $r'(x)$ in the same manner. This yields

$$\tilde{p}(r, \theta, t) = \tilde{A}_0 \sum_{n=1}^{M} \int_{-l/2}^{l/2} \frac{1}{r'_n} \mathrm{e}^{\mathrm{j}(\omega t_n - kr'_n)} \, \mathrm{d}x_n. \tag{13}$$

Here the subscript n denotes the dependence on the particular coordinate system. The parameter $l = L/M$ represents the length of the individual element, which is identical to the spacing between centers of adjacent elements.

For each partial integral we can make the far-field assumption that $r'_n \gg l$ so that $1/r'_n \approx 1/r_n$ and $\exp(-\mathrm{j}kr'_n) \approx \exp[-\mathrm{j}k(r_n - x_n \sin\theta_n)]$. Also we are free to rename the integration variable x_n as x,

$$\tilde{p}(r, \theta, t) = \tilde{A}_0 \sum_{n=1}^{M} \frac{1}{r_n} \mathrm{e}^{\mathrm{j}(\omega t_n - kr_n)} \int_{-l/2}^{l/2} \mathrm{e}^{\mathrm{j}kx \sin\theta_n} \, \mathrm{d}x. \tag{14}$$

After that we can solve the partial integrals and obtain

$$\tilde{p}(r, \theta, t) = \tilde{A}_0 l \sum_{n=1}^{M} \frac{1}{r_n} \mathrm{e}^{\mathrm{j}(\omega t_n - kr_n)} \frac{\sin\left(\frac{1}{2} kl \sin\theta_n\right)}{\frac{1}{2} kl \sin\theta_n}. \tag{15}$$

Obviously this sum can be understood as a set of point sources with the directivity function

$$\tilde{\Gamma}(\theta) = \frac{\sin\left(\frac{1}{2} kl \sin\theta\right)}{\frac{1}{2} kl \sin\theta}. \tag{16}$$

This proves that Eq. (11) also applies when a continuous line source is subdivided into smaller line sources. But it is only valid in the far field of the partial source.

Note that this derivation does not incur any loss of generality. The concept of subdividing the given integral and solving for the far field of the individual element is fully applicable to any continuous one-dimensional source, such as curved lines.

Examples The following four figures demonstrate the applicability of the CDPS decomposition using a few selected examples. All of them show vertical polar plots of the radiation of an ideal (vertical) line source at a

radial scale of 40 dB. In all cases we compare the solution provided by the CDPS model [Eq. (15)] with the detailed numerical solution [Eq. (7)] of the original integral [Eq. (1)].

Fig. 2 shows the reproduction of a continuous source of 1-m length by four point sources with complex directivity data at a measurement distance of 3 m. Although the spacing of 0.25 m between the elements is significantly larger than the half-wavelength at 2 kHz, the match is very good. Fig. 3 shows the same setup at a measurement distance of 1.5 m. At this distance the measurement point begins to move into the near field of the individual element. Accordingly deviations begin to appear. In contrast, Fig. 4 shows the same configuration and distance but now using eight elements with a size/spacing of 0.125 m. Obviously an exact match is reestablished because the far-field condition is fulfilled again. Finally Fig. 5 shows

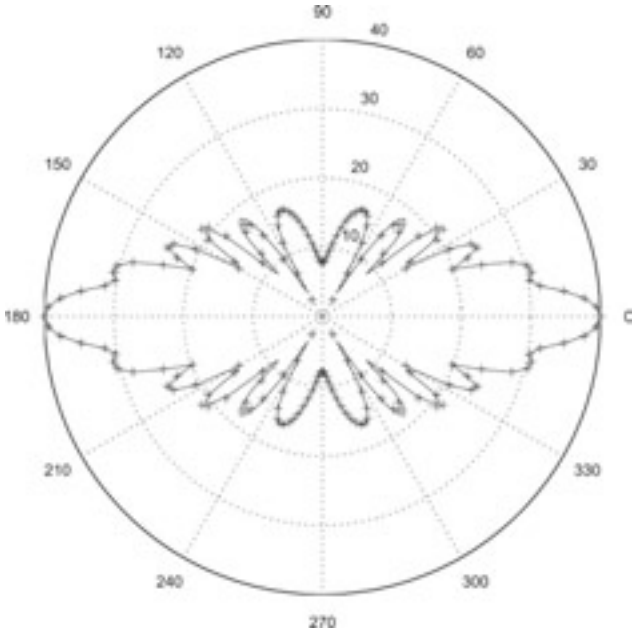

Fig. 2. Comparison of line source integral (—) with approximation by four point sources with complex directivity (+++). $f = 2$ kHz, $r = 3$ m, $L = 1$ m. Note that spacing $l = 0.25$ m is larger than wavelength $\lambda = 0.17$ m.

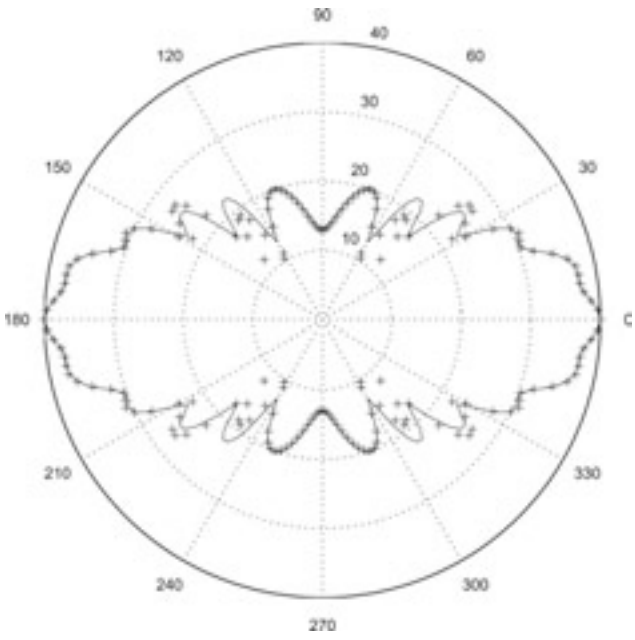

Fig. 3. Comparison of line source integral (—) with approximation by four point sources with complex directivity (+++). $f = 2$ kHz, $r = 1.5$ m, $L = 1$ m. Note that at 1.5 m we are entering the near-field zone of the individual source.

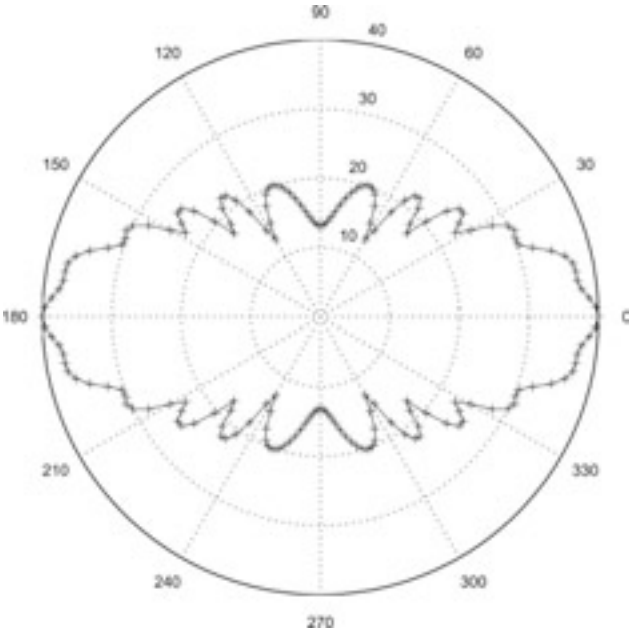

Fig. 4. Comparison of line source integral (—) with approximation by eight point sources with complex directivity (+++). $f = 2$ kHz, $r = 1.5$ m, $L = 1$ m. At 1.5 m an element size $l = 0.125$ m is sufficient.

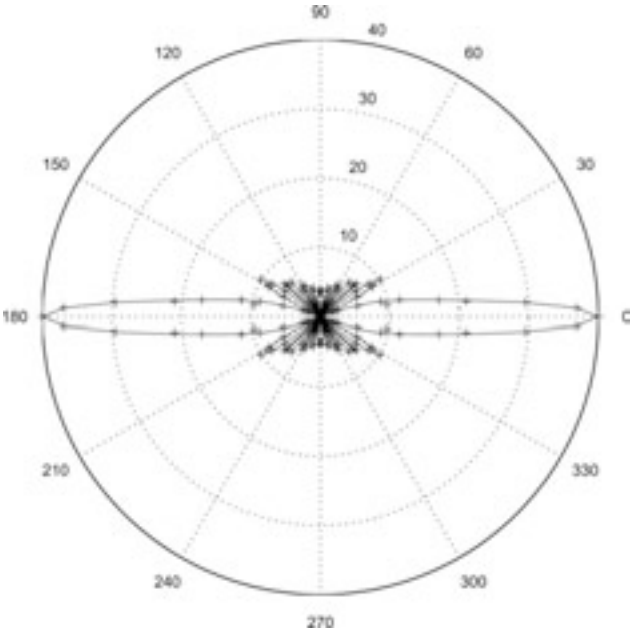

Fig. 5. Comparison of line source integral (—) with approximation by four point sources with complex directivity (+++). $f = 10$ kHz, $r = 8$ m, $L = 1$ m. Width and size of main lobe are well reproduced with an element spacing $l = 0.25$ m, even at wavelength $\lambda = 0.034$ m.

a different setup, namely, the comparison of four elementary sources using complex directivity data with the exact solution at a frequency of 10 kHz and a distance of 8 m. As can be seen clearly, main lobe and substructures match very well, although the element spacing is an order of magnitude larger than half the wavelength λ/2.

2.2.2. Data Requirements

In order to describe a line source as characterized by Eq. (3) or Eq. (15) by the discretized CDPS model [Eq. (10)], a set of conditions must be fulfilled. These originate in the specific properties of the line source, but similar requirements are found for the far-field solution of other types of continuous sources.

Complex Directivity Data First of all, phase data must be included. This can be seen immediately from Eq. (16) because $\tilde{\Gamma}(\theta) \neq |\tilde{\Gamma}(\theta)|$. The phase over angle θ or frequency f is basically a step function that switches between two states, 0 and π, at every zero of the directional factor. Omitting this information will lead to erroneous results when computing the linear superposition of multiple sources.

This is illustrated by Fig. 6, which shows the magnitude and phase of the vertical polar response for a line source of 1-m length at 2 kHz in the far field. Note that the phase was compensated for the propagation delay and normalized so that a phase value of 180° equals the polar origin, and 0 equals 38 dB.

Angular Resolution Eq. (16) also gives an idea about the angular resolution required for the discrete point-source model [Eq. (10)]. Based on the directional factor we can derive the angular spacing of the off-axis nulls, where $\tilde{\Gamma}(\theta) = 0$. From there it is only a small step to define the angular resolution needed for an accurate description by the directivity matrix $\hat{A}$.

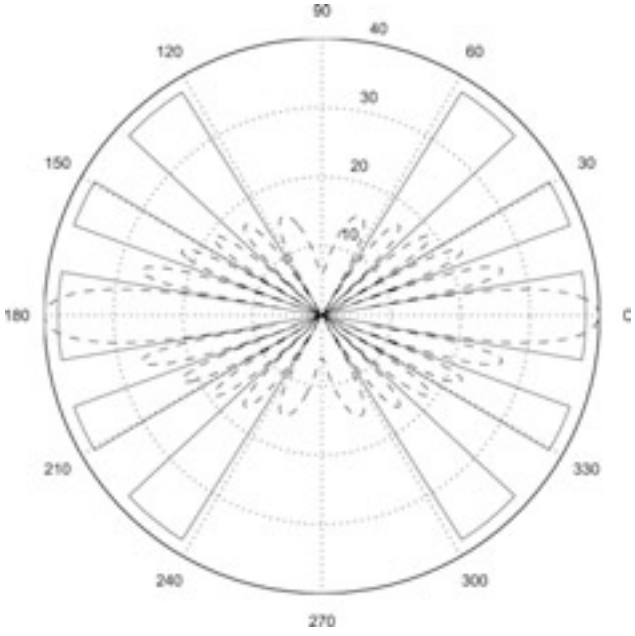

Fig. 6. Magnitude (- - -) and phase (—) of an ideal, finite line source of length $L = 1$ m, at $f = 2$ kHz, in the far field. Phase was scaled so that 38 dB is equivalent to 0°. Note that phase switches at every minimum.

The nulls of the angle-depending directional factor are distributed according to

$$\theta_i = \arcsin\left(\pm i\frac{c}{fl}\right), \qquad i = 1, 2, \ldots . \tag{17}$$

Here θ_i denotes every angular location i where the directional factor vanishes. As an example, for a source length $l = 0.2$ m, a frequency $f = 10$ kHz, and a speed of sound $c = 340$ m/s the first null occurs at $\theta_1 \approx 10°$, the second at $\theta_2 \approx 20°$. For shorter sources the spacing of nulls becomes wider for the same frequency (Table 1).

In order to avoid aliasing or undersampling errors, the angular resolution must be high enough given the length of the source l and the upper frequency limit. This resolution limit can be approximated by half the angular distance between the first and second minimum,

$$\Delta\theta_{\text{crit}} = \frac{1}{2}\left[\arcsin\left(2\frac{c}{fl}\right) - \arcsin\left(\frac{c}{fl}\right)\right]. \tag{18}$$

For this example an angular resolution of 5° could be just sufficient. In general angular resolutions of $\Delta\theta \leq \Delta\theta_{\text{crit}}$ should be used (Table 2).

Indeed, in practice another issue is equally important. Because the main lobe (on axis, $\theta = 0°$) becomes very tight for high frequencies, the on-axis data must be captured carefully in order to obtain the actual on-axis level. This is especially important for turntable measurements. Table 3 shows some exemplary data calculated from Eq. (16) for angles θ close to 0°.

A small angular deviation from the exact on-axis direction will result in a lower on-axis level measurement,

Table 1. Angular locations of minima 1–5 for different source lengths l at frequency $f = 10$ kHz.

Length l, m	0.1	0.2	0.4	0.8
θ_1	19.9°	9.8°	4.9°	2.4°
θ_2	42.8°	19.9°	9.8°	4.9°
θ_3	—	30.7°	14.8°	7.3°
θ_4	—	42.8°	19.9°	9.8°
θ_5	—	58.2°	25.2°	12.3°

Table 2. Minimum required angular resolutions for different source lengths l at frequency $f = 10$ kHz.

Length l, m	0.1	0.2	0.4	0.8
$\Delta\theta_{\text{crit}}$	10°	5°	2.5°	1°

Table 3. Attenuation at off-axis angles compared to on axis for different source lengths l at frequency $f = 10$ kHz.

Length l, m	0.1	0.2	0.4	0.8
Level at 1°, dB	−0.04	−0.15	−0.61	−2.56
Level at 2°, dB	−0.15	−0.61	−2.56	−13.7
Level at 3°, dB	−0.34	−1.40	−6.32	—

because the pressure function changes quickly with the angle. Failing to measure the correct level of the maximum will increase the level of the sidelobes artificially and thus lead to erroneous results later on.

Frequency Resolution Similar to the angular resolution we can derive a condition for the needed spectral resolution from Eq. (16). In the frequency domain the spacing of nulls corresponds to

$$f_i = i\frac{c}{l\sin\theta}, \qquad i = 1, 2, \ldots \tag{19}$$

where f_i denotes the frequencies i for which the directional factor becomes zero. For the example of $l = 0.2$ m and $c = 340$ m/s the frequency nulls occur at a spacing of 1700 Hz when considering an angle of $\theta = 90°$. The spacing is larger for smaller angles and for smaller source lengths. Table 4 shows some exemplary data.

In order to resolve the spectral structure we have to define the condition

$$\Delta f_{\text{crit}} = \frac{c}{2l\sin\theta} \tag{20}$$

which means that in order to avoid aliasing problems there should be at least two data points for every frequency section enclosed by adjacent zero points of the directional factor. This corresponds to minimum required frequency resolutions $\Delta f \le \Delta f_{\text{crit}}$.

The highest resolution requirement occurs for $\theta = 90°$,

$$\Delta f_{\text{crit}} = \frac{c}{2l} \tag{21}$$

which corresponds to 170 Hz for a 1-m line source. We remark that practically all modern FFT-based measurement systems provide frequency resolutions that are much higher than this.

Frequency Averaging In acoustics the frequency resolution is often based on fractional octave bands. It is important to understand when it is valid to average data such as the modulus of the directional factor over a bandwidth.

One can imagine that the average over a frequency range that includes less than half the spectral distance between two nulls [Eq. (19)] can be used as a representative value. That is possible because the average will not depend much on the actual limits of the averaging bandwidth but rather follow the underlying function smoothly. On the other hand, if the average is computed over a frequency bandwidth of at least twice the angular distance between two minima one can assume that the average will be representative as well. The reason is that for a large enough bandwidth additional variations of the underlying function will not be significant.[1] But for the intermediate frequency range small variations of the limits of the averaging bandwidth will lead to large variations of the average value, which in turn leads to meaningless data. This is the "forbidden" frequency range. Figs. 7 and 8 show examples for a bandwidth of one-third octave.

Given a bandwidth b in fractional octaves we can calculate the exact center frequency of the related band that has the width of the linear frequency resolution Δf,

$$f_c = \frac{\Delta f}{2^{b/2} - 2^{-b/2}}. \tag{22}$$

Based on this we can determine directly for which frequencies f_c and fractional octave resolutions b averaging is allowed. For the lower frequency limit the linear resolution in Eq. (22) is given by half the spacing of minima according to Eq. (20),

$$f_{\text{lower}} = \frac{c}{2l\sin\theta}\frac{1}{2^{b/2} - 2^{-b/2}}. \tag{23}$$

The upper frequency limit is given by twice the spectral spacing between minima,

$$f_{\text{upper}} = \frac{2c}{l\sin\theta}\frac{1}{2^{b/2} - 2^{-b/2}} = 4f_{\text{lower}}. \tag{24}$$

In the intermediate range of $f_{\text{lower}} < f_c < f_{\text{upper}}$ the frequency data points are too coarse and will generate aliasing errors due to the quickly varying average that is sampled using points that are too far apart.[2]

As an example, for $l = 0.2$ m, $c = 340$ m/s, $\theta = 90°$, and a resolution of one-third-octave bandwidth $b = 1/3$, data can be averaged meaningfully below 3670 Hz and above 14 700 Hz (Fig. 7). If the length of the source is greater, these frequency limits will be reduced. They will be increased when looking at smaller angles.

A selection of different values is shown in Table 5. It is obvious that the forbidden frequency range depends strongly on the angle and can thus not be understood as a fixed range for a given source length l. In general, one can derive two different regimes.

- For large sources ($l > 2$ m) averaging over wide bandwidths, such as 1/1 octave, may be useful to derive representative data in a statistical way.
- For small to medium size sources ($l < 0.5$ m) averaging over small bandwidths, such as 1/24 octave or 1/36 octave, may be used to smooth the frequency response curve without losing significant information.

Table 4. Frequencies of minima 1–5 for different source lengths l at frequency $f = 10$ kHz and angle $\theta = 90°$.

Length l, m	0.1	0.2	0.4	0.8
f_1, Hz	3400	1700	850	425
f_2, Hz	6800	3400	1700	850
f_3, Hz	10 200	5100	2550	1275
f_4, Hz	13 600	6800	3400	1700
f_5, Hz	17 000	8500	4250	2125

[1]The choice of half or twice the spacing between adjacent minima as a condition seems natural but is somewhat arbitrary. Of course, higher requirements will lead to smaller quantitative errors.

[2]The potential error can be quantified by approximating the band average of Eq. (16) and analyzing its variations over the frequency range.

For intermediate averaging bandwidths, such as one-third octave, most data will suffer from significant sampling errors. That can only be avoided for carefully selected angles and frequencies of interest. As an example Fig. 8 displays the frequency response of Fig. 7 smoothed to one-third octave. In the forbidden range the distance between one-third octave center frequencies is too large to capture the fundamental behavior of the average function. In this case variations of up to 6 dB occur between adjacent data points.

Figs. 9 and 10 emphasize these findings on the basis of real-world measurements. They show the off-axis frequency response of a ribbon loudspeaker (Alcons

Table 5. Forbidden frequency ranges, in Hz, for different source lengths l, fractional octave bandwidths b, and angles θ.

	$l = 0.2$ m		$l = 0.8$ m	
Bandwidth b	f_{lower}	f_{upper}	f_{lower}	f_{upper}
1/1 at $\theta = 20°$	3500	14 000	900	3500
1/3 at $\theta = 20°$	10 700	43 000	2700	10 700
1/24 at $\theta = 20°$	86 000	344 000	21 500	86 000
1/1 at $\theta = 60°$	1400	5600	350	1400
1/3 at $\theta = 60°$	4200	17 000	1100	4200
1/24 at $\theta = 60°$	34 000	136 000	8500	34 000

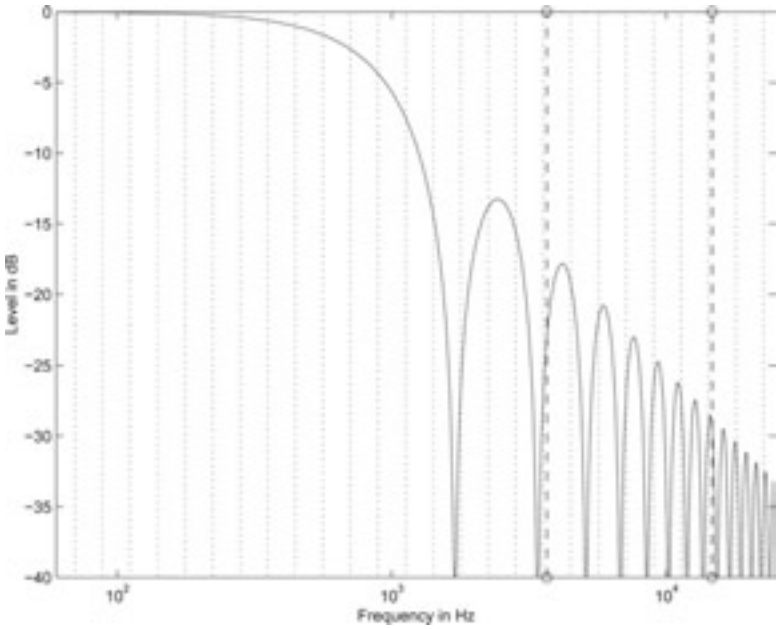

Fig. 7. Frequency response (—) of ideal line source of length $l = 0.2$ m at an angle of 90° off axis in the far field. (· · ·) bands of one-third-octave width, (- - -) forbidden range from 3670 to 14 700 Hz.

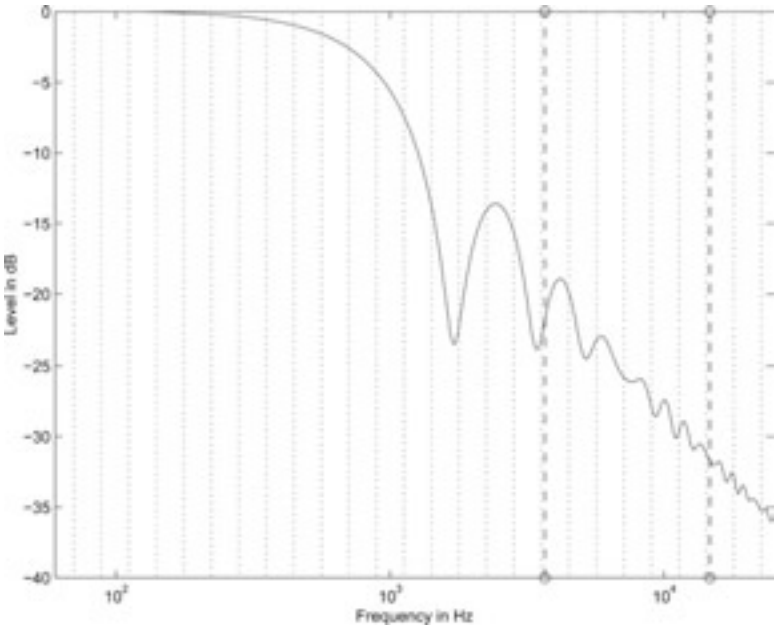

Fig. 8. Smoothed frequency response (—) of ideal line source of length $l = 0.2$ m at an angle of 90° off axis in the far field. Smoothing bandwidth is one-third octave. (· · ·) bands of one-third-octave width, (- - -) forbidden range from 3670 to 14 700 Hz.

Audio QR18, 0.5 m tall) at a vertical angle of 50°. In Fig. 9 minima are indicated by cursor lines. They seemingly match with the expected frequency response. The spacing of nulls should be about 890 Hz at this angle. Fig. 10 presents a continuous one-third-octave band frequency average of the measured response. This is to show that in the forbidden range of 2–8 kHz data sampled in one-third-octave steps have little meaning. Over this frequency range the variations of the curve are too large and sampling errors on the order of 6 dB can occur.

We remark that similar considerations with respect to resolution and averaging also apply to loudspeakers with a crossover, which can be regarded as very small line arrays in the frequency range of the crossover.

Finally we need to emphasize that the preceding discussion regarding frequency averaging is only concerned with magnitude data. If sources are to be combined coherently, one will need to take care of phase data as well. However, especially for a line source, averaging phase data over a frequency bandwidth that contains a minimum leads to arbitrary results because of the switching behavior of the phase function [Eq. (16)].

Measurement Distance With respect to the measurement distance we emphasize that the CDPS model is only

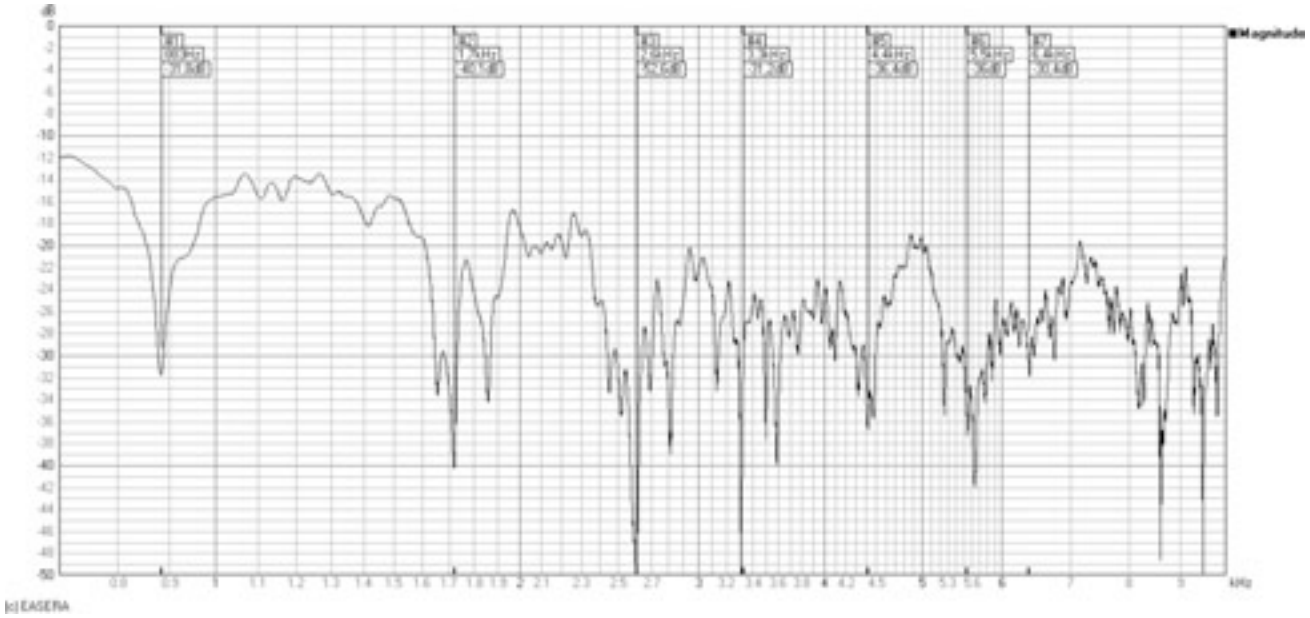

Fig. 9. Frequency response of AlCons Audio QR18 loudspeaker at 50° off axis normalized to 0°. Cursors denote minima of corresponding ideal line source.

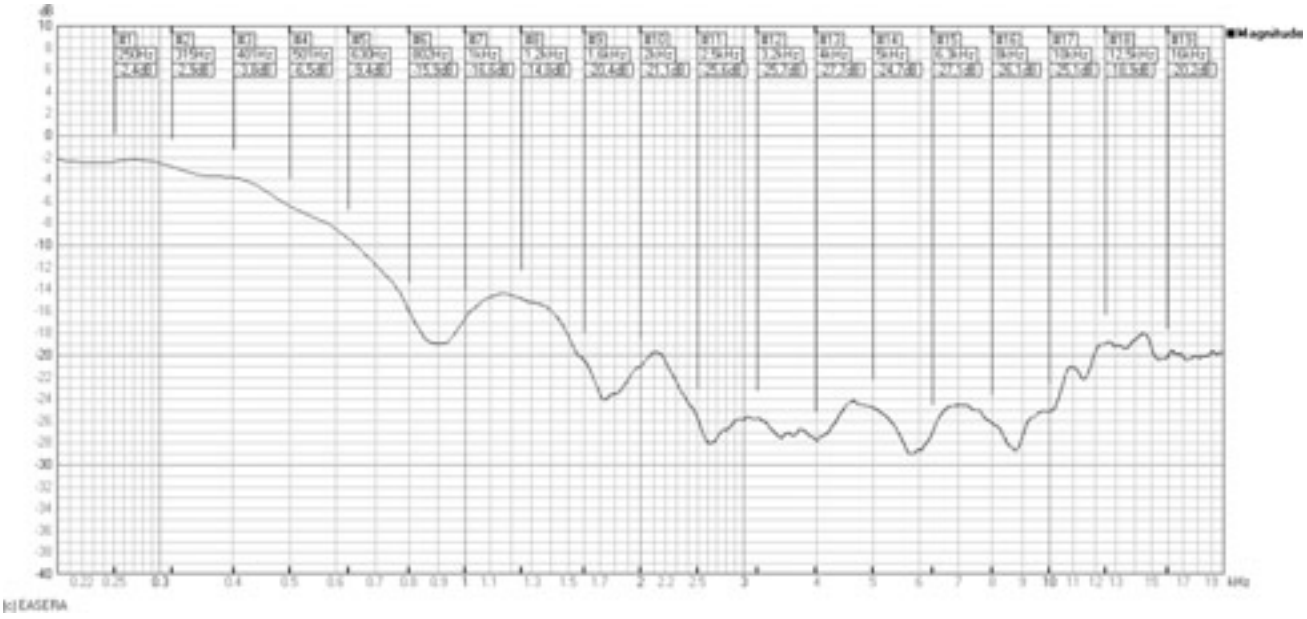

Fig. 10. Frequency response of AlCons Audio QR18 loudspeaker at 50° off axis normalized to 0° and smoothed at one-third-octave bandwidth. Cursors denote center frequencies of standardized one-third-octave bands.

valid in the far field of the particular source. This applies to both measurement and prediction. Measurements of the sources must be taken in the corresponding far field. Calculation results will only be valid at points in the approximate far field of the modeled source (see also Figs. 2–4 and [14]).

However, we would like to emphasize once more that this is typically not the far field of the entire device. A line source may be subdivided into elements, for each of which the far-field condition must hold. But nevertheless the near field of the line source as a whole can be modeled correctly.

3 VALIDATION

In this section we will apply the CDPS model to a typical line array system. Validation will be based on the comparison of measurement data for the entire array with modeling results for the array based on the far-field measurements of the individual cabinets. We will be mostly concerned with the frequency response and the polar data in the vertical domain.

3.1 Small Installation Line Array

3.1.1. Overview

A curved array of 12 Martin Audio Omniline cabinets [22] was used for this comparison, as depicted in Fig. 11. The overall size of a cabinet is 0.12 m, the length of the array is about 1.4 m.

Isolated Model First we predict the performance of the complete system by using balloon measurements of a single isolated cabinet. Although the match between measurement and prediction turns out to be already satisfying, it is clear that this method of modeling the individual point sources cannot account for acoustic support and shadowing effects caused by cabinets adjacent in the array.

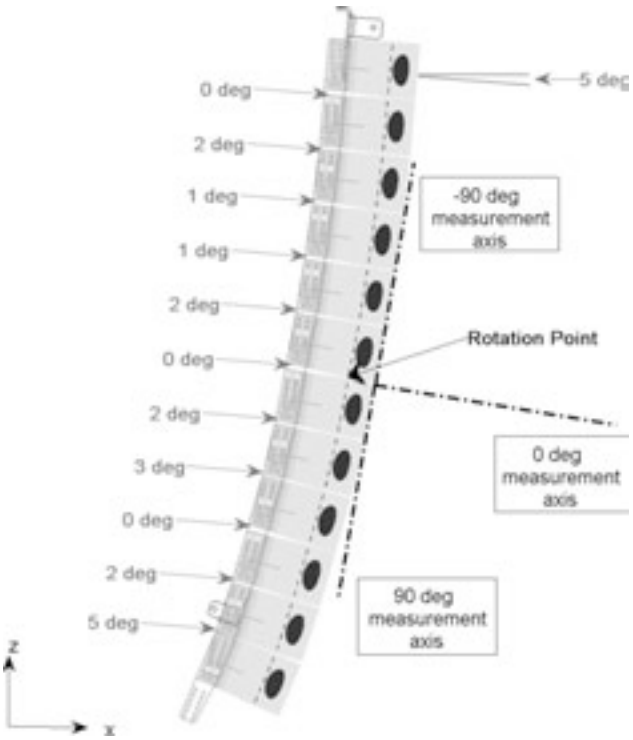

Fig. 11. Polar measurement setup and array configuration.

Flanked Model Results can be improved when the balloon data of a cabinet are acquired with the top and bottom neighbors in place. Although the two outer cabinets will be switched off and electrically short-circuited, they will contribute indirectly to a more realistic radiation behavior for the representative point source. We will call this the flanked case and show that the average deviation between measurement and simulation decreases compared to the isolated case.

An example is given in Fig. 12(a) and (b), where the vertical directivity maps for the isolated and flanked cases are shown. The level attenuation relative to the on-axis direction is displayed as a function of frequency and angle.

Positional Model Consideration of the rules of superposition inevitably leads to a second step of improvement. One should think that the acoustic radiation characteristics of the outer cabinets in the array, especially the very top and bottom elements, will be different from the ones in the center. In consequence, another significant improvement can be reached by using different balloon data for different cabinet positions in the array. This will be the positional model. Such data can be measured as well, though suitably accurate mechanical positioning methods of an array with a weight of possibly some hundreds of kilograms, often with the center of gravity distant from the rotation point, do not exist.

The boundary-element method (BEM) [23] provides us with a method of placing neighboring unexcited elements around the active element and acquiring complex pressure on any three-dimensional surface around that element. Previous studies had shown that when the elemental source has high enough directivity the isolated measurement is valid [24]. Also it was shown that the radiation behavior of a lower box is very close to that of a mirrored version of the corresponding upper box and that central boxes share similar radiation characteristics.

In this study elemental complex spherical data were obtained for the top four boxes of a typically curved 12-box array over the full bandwidth of the low/mid driver. An average of the centrally positioned box data was also obtained, resulting in five independent data sets. As an example, Fig. 12(c) and (d) shows the vertical directivity maps as utilized for the topmost element and the central elements.

The validity of the data at increased distances has been checked by calculating the balloons at diameters of up to 32 m in BEM. The balloon data sets for various diameters show very minor deviations with increasing distance (less than 1 dB at distances of up to 32 m).

We could have measured isolated elemental data for the high-frequency sections of the system. However, BEM was applied to the high-frequency horn of an isolated box with a simplified driving surface. The reason, apart from the data already existing as part of the design process, was that we free ourselves from the usual measurement errors, such as position uncertainty and environmental factors. This advantage is particularly apparent at high frequencies.

3.1.2 Frequency Response

Fig. 13(a) shows the measured absolute sensitivity of the line array compared to the results predicted by the three different models. At first glance one can already see that the isolated model shows the largest deviations whereas the flanked and positional models appear to be much closer. This becomes clearer in the relative display of Fig. 13(b), where the sensitivity data are normalized to the measurement. For the on-axis direction the isolated case shows an average error of about ±3 dB, with maximum errors of up to 6 dB. The prediction based on the flanked setup is typically within ±2 dB, with peak errors of maximally 3 dB. The best match is reached when accounting for the position of a cabinet in the array. Here the error is about ±1 dB on average, with peaks of about 2 dB. A similar picture is given in Fig. 13(c) where the error is averaged over a set of 41 data points, namely, the relative errors within an opening angle of ±20°.

The largest errors seem to occur in three fairly separate frequency ranges.

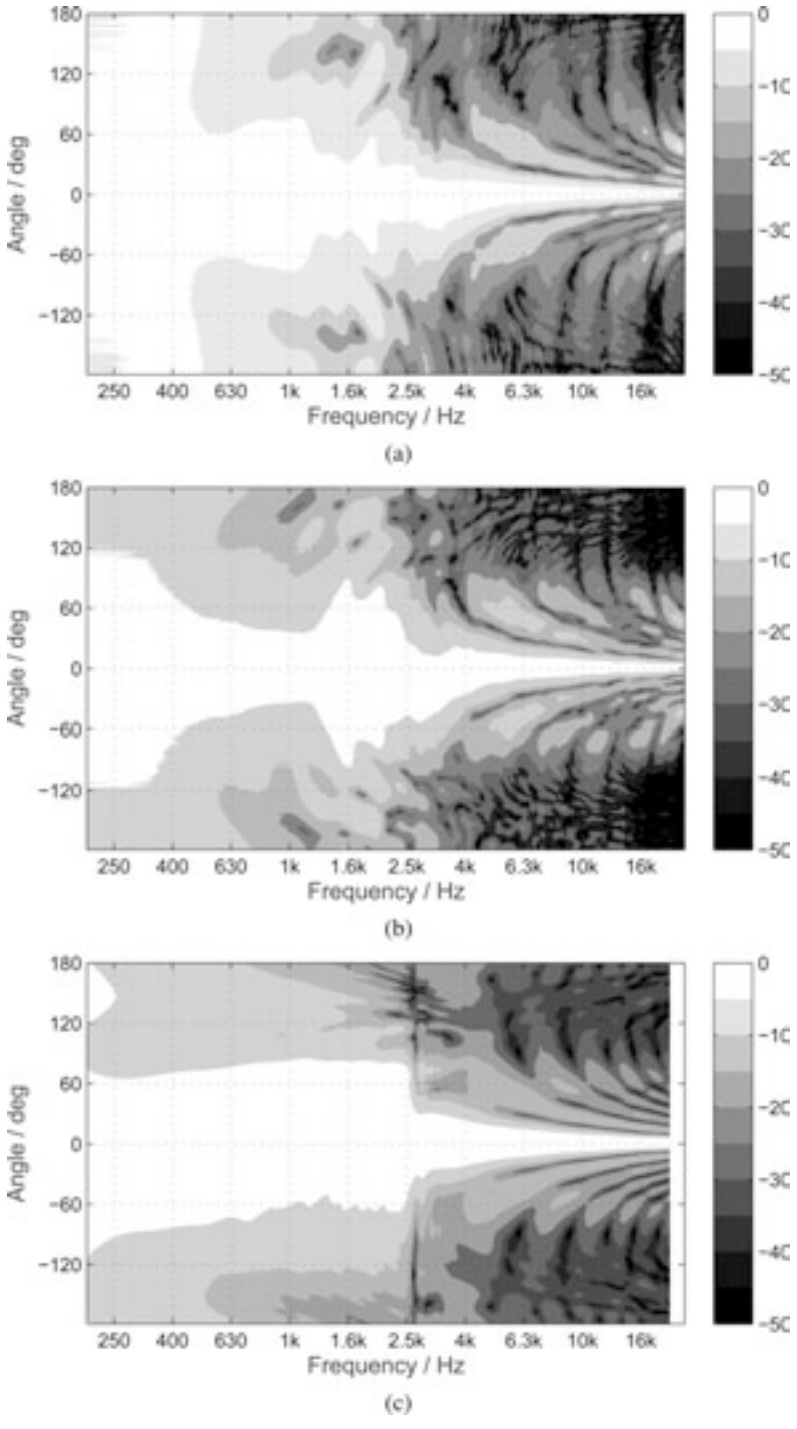

Fig. 12. Vertical directivity maps. (a) Measured line array cabinet, isolated case. (b) Measured line array cabinet, flanked case. (c) Topmost cabinet in line array, BEM modeled, positional case. (d) Averaged center cabinets of line array, BEM modeled, positional case.

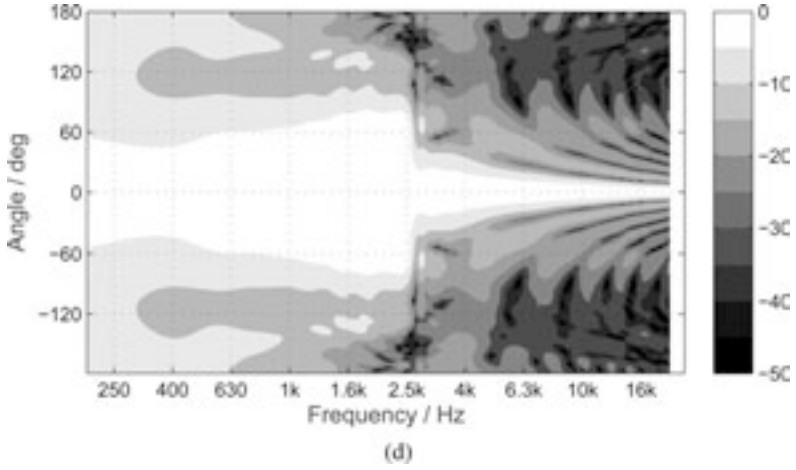

(d)

Fig. 12. *Continued*

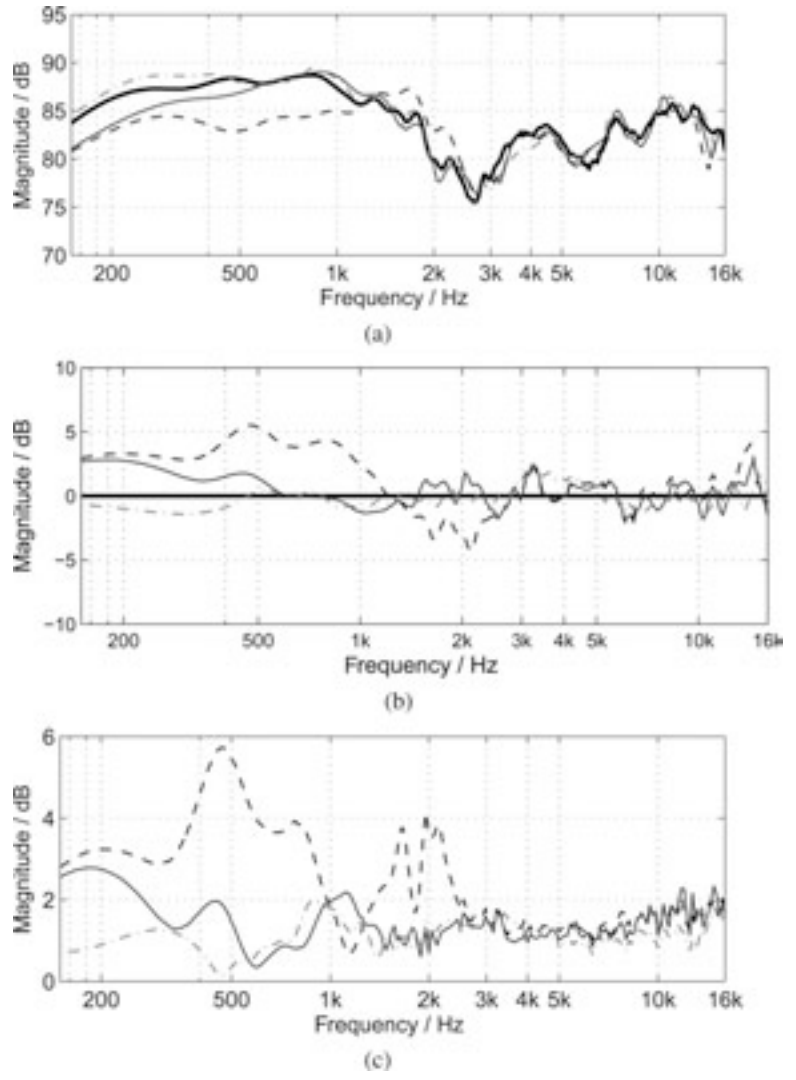

(a)

(b)

(c)

Fig. 13. (a) Measured sensitivity of line array (—) compared to predicted sensitivity, isolated (- - -), flanked (—), and positional (- · -). (b) Predicted sensitivity of line array relative to measurement (—), isolated (- - -), flanked (—), and positional (- · -). (c) Predicted sensitivity of line array relative to measurement, averaged over an opening angle of ±20°, isolated (- - -), flanked (—), and positional (- · -).

- In the low-frequency range of about 500 Hz shadowing and acoustic support effects by neighbor elements in the array seem to be particularly dominant. Since the isolated model cannot model that, it shows the largest deviations. The positional model is better in this respect.
- In the mid-frequency range of 2–4 kHz, where the crossover is located, deviations are larger for all models. The isolated case being much worse, again due to a lack of interference from nearby irradiated surfaces, there is not a big difference between flanked and positional models. We will see later that this is the region of maximum elemental response deviation. A contribution to this error likely depends on the measurement accuracy of the elements and the prediction accuracy of the array, which is normally lower in the crossover range. That is because the number of interacting sources basically doubles, and accordingly the inherent elemental measurement errors increase the overall error of the simulation.
- In the very high-frequency range above 10 kHz deviations increase again. This has to be expected since the measurement accuracy, and thus the prediction accuracy, becomes lower at very small wavelengths. Finite spatial accuracy and the influence of environmental factors during the measurement introduce noise and inaccuracy, especially into the phase data, which propagate through the prediction.

3.1.3 Polar Response

Fig. 14 compares the polar responses of measured and predicted arrays for the isolated case. Analogously, Figs. 15

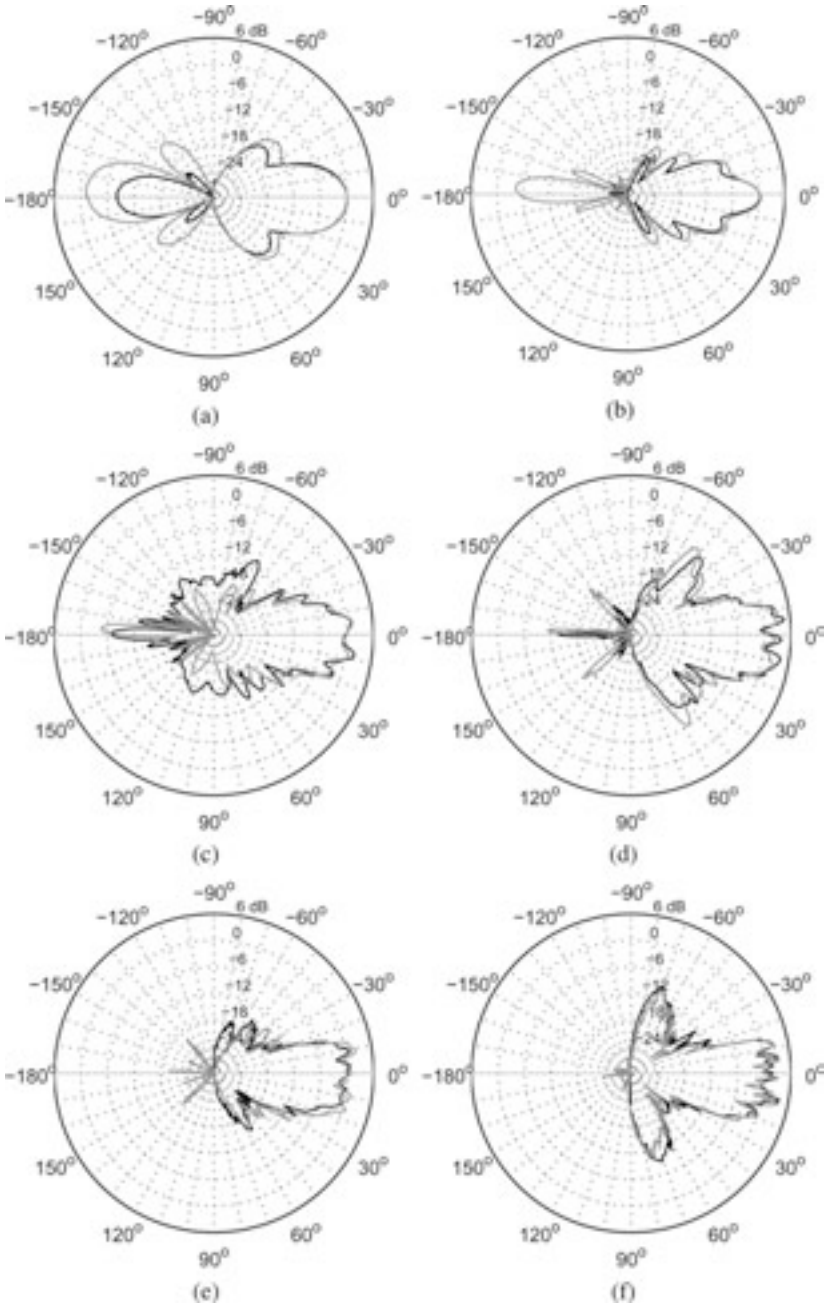

Fig. 14. Vertical polar plots of line array, isolated case (—) compared to measurement (—), (a) 500 Hz, (b) 1 kHz, (c) 2 kHz, (d) 4 kHz, (e) 8 kHz, (f) 16 kHz.

and 16 show overlays of the predicted vertical polar responses with measurements for the flanked and positional cases, respectively. These data were acquired from 100 Hz to 20 kHz and are displayed on graphs with a 36-dB radial scale. The angular scale denotes 0° for the on-axis direction and −90° for the upward direction. For better comparison the data were smoothed to one-sixth-octave bandwidth.

First we can state that all models match quite well with the measurements. Qualitatively the line array behavior is reproduced very well over the entire frequency range. Similar to the frequency response before, there is an increase in overall accuracy for the flanked model and, especially, for the positional model.

Naturally, errors are smaller for the front than for points on the backside of the array. Although still being linear, interaction effects on the backside of the cabinets cannot be predicted so precisely using the assumption of coherent point sources. Typically one has to expect rather an intermediate state between full coherence and random phase. This error results in less pronounced extrema, both minima and maxima, in the measurement compared to the prediction.

Deviations for the low-frequency range at about 500 Hz have the same reason as explained in the frequency response considerations. The second most obvious differences between measurement and computation occur in the crossover range between 2 and 4 kHz, where the first sidelobes are reproduced with an error of about 3 dB. This effect will be investigated further in the following subsection.

Finally we recognize that the positional model shows some stronger deviations at very high frequencies for off-

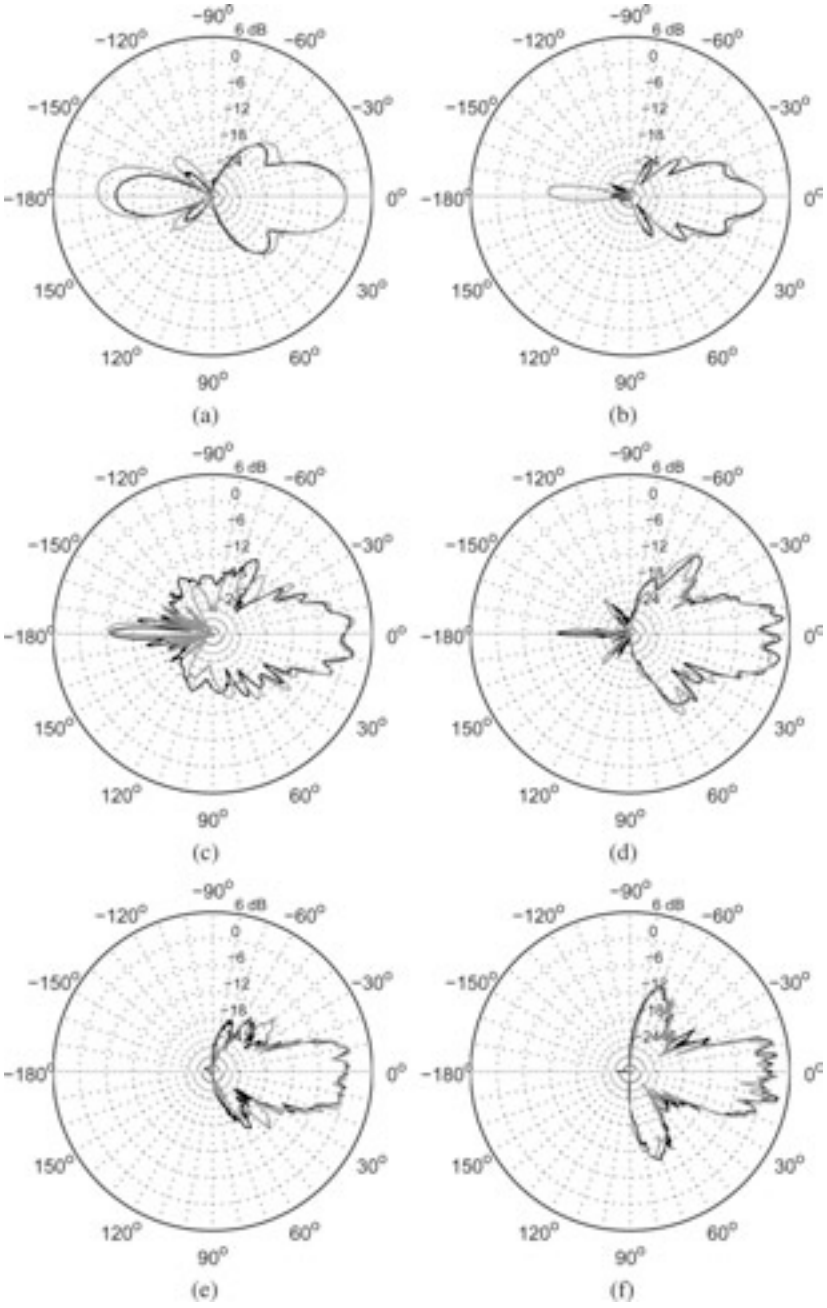

Fig. 15. Vertical polars of line array, flanked case (—) compared to measurement (—), (a) 500 Hz, (b) 1 kHz, (c) 2 kHz, (d) 4 kHz, (e) 8 kHz, (f) 16 kHz.

axis angles of about 80°. Especially the main sidelobe at 16 kHz is better reproduced by the isolated and flanked models than by the positional model. This is due to the simplified nature of the driving source in the BEM model. A more representative source could be modeled that would replicate the very high-frequency aliasing components if desired.

3.1.4 Elemental Deviation

So far we have assumed that the individual cabinets used in the array have identical axial sensitivities. However, in practice there are some variations between individual samples. Fig. 17(a) shows the deviations of the frequency responses of the 12 different cabinets from the mean of the set. Over the largest part of the frequency range the cabinets fall within a variation of about ±1 dB. Only in the crossover range larger deviations of up to 3 dB occur. Fig. 17(b) displays a similar plot for the on-axis phase responses. The variation is approximately ± 6° with peaks of up to 30° in the crossover range.

To better understand the effects of these errors, we corrected the respective point sources to incorporate the deviations and once more modeled the whole array. Fig. 17(c) shows the resulting deviations between measurement and prediction. Compared to Fig. 13(c) the behavior seems to be largely unaltered. But a closer look at the crossover range reveals that particularly in this sensitive region the error had decreased notably, on average by about 0.5 dB. This is most obvious in Fig. 17(d), which quantifies the improvement relative to the measurements when using elemental corrections.

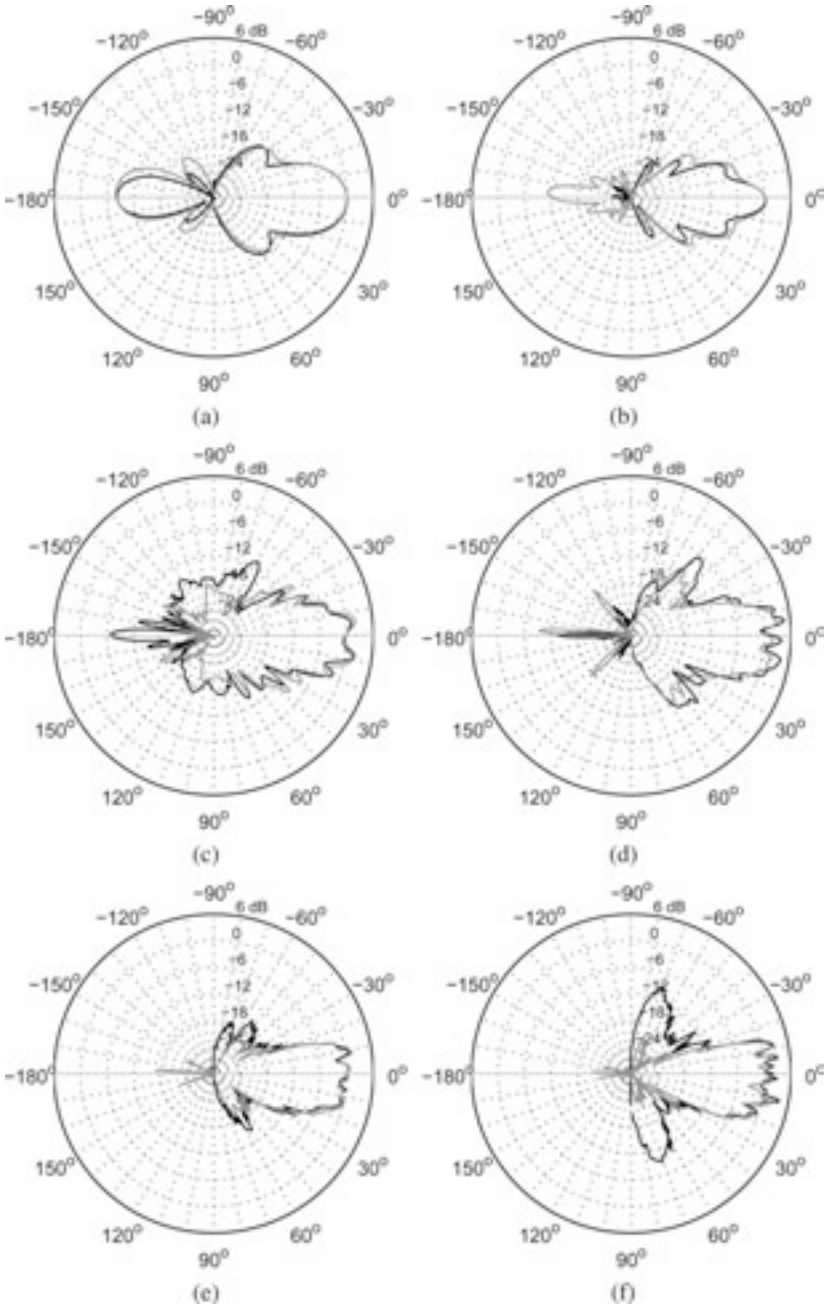

Fig. 16. Vertical polars of line array, positional case (—) compared to measurement (—), (a) 500 Hz, (b) 1 kHz, (c) 2 kHz, (d) 4 kHz, (e) 8 kHz, (f) 16 kHz.

The same effect is shown in Fig. 18, where the polar data from 2–4 kHz are presented for each model—isolated, flanked, and positional. Compared to the original polar response comparison the match seems to be much better now, especially the small sidelobes are reproduced clearly.

Of course we have to state that this finding is of not much immediate practical value. In reality it is typically not possible to measure the on-axis responses of all concerned loudspeaker cabinets for prediction purposes. This is especially true when an installation is still being planned and the particular loudspeakers are not even

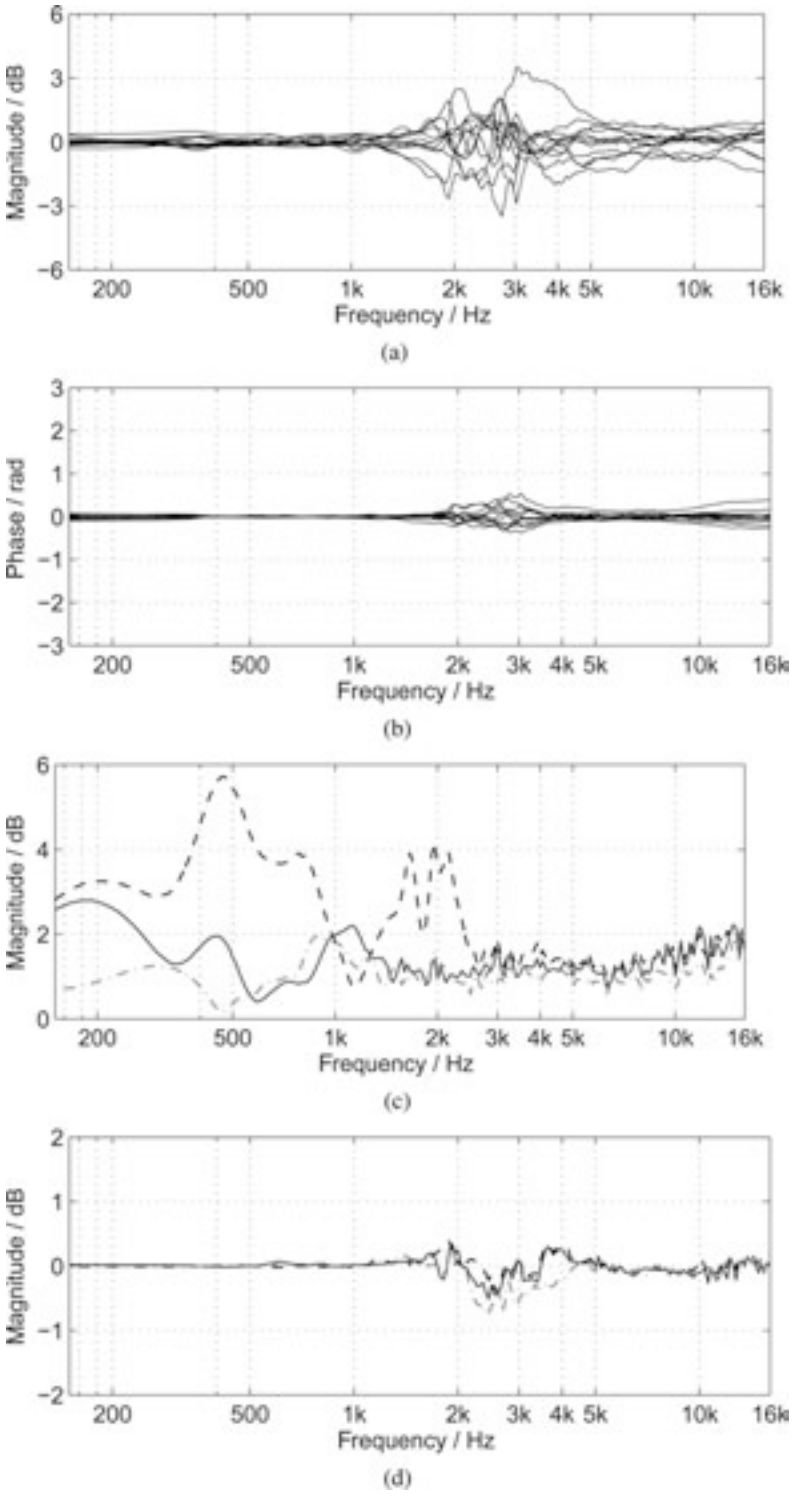

Fig. 17. (a) Elemental magnitude deviation of on-axis response at 1 m, relative to mean of set. (b) Elemental phase deviation of on-axis response at 1 m, relative to mean of set. (c) Predicted sensitivity of line array relative to measurement using elemental complex on-axis corrections, averaged over an opening angle of ± 20°. (- - -) isolated, (—) flanked, (- · -) positional. (d) Relative improvement of predicted sensitivity when using elemental complex on-axis corrections. Change of sensitivity shown in Fig. 13(c) compared to Fig. 17(c). (- - -) isolated, (—) flanked, (- · -) positional.

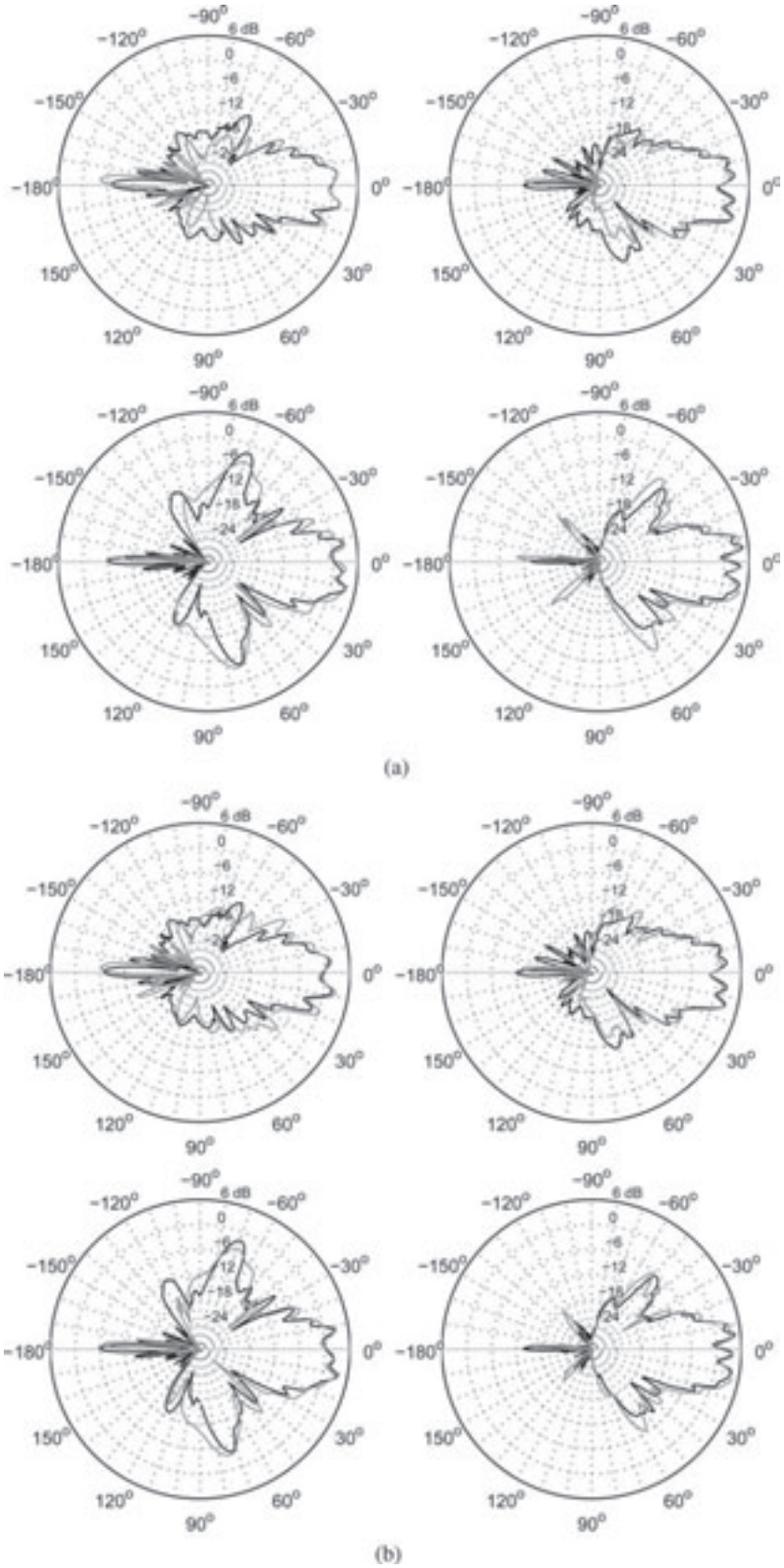

Fig. 18. Vertical polar plots of line array from top left to bottom right: 2 kHz, 2.5 kHz, 3.15 kHz, 4 kHz. (a) Isolated case (—) compared to measurement (**—**) using elemental complex on-axis corrections. (b) Flanked case (—) compared to measurement (**—**) using elemental complex on-axis corrections. (c) Positional case (—) compared to measurement (**—**) using elemental complex on-axis corrections.

available yet. Nevertheless one gains good insight into the effect of sample-to-sample variations on the prediction accuracy for a full array. Surprisingly it is not as large as one would expect using simple methods of error propagation. On the other hand, this quantifies the potential accuracy gains in the simulation that can be obtained by improvements with regard to production tolerance.[3]

We add that so far we have not compared full balloon data for different cabinet samples. However, it is likely that the axial deviation is dominant compared to the variations in the polar response.

3.2 Medium-Size Touring Line Array

3.2.1 Overview

Several comparisons were made using the SEQUENZA 10 line array from Kling & Freitag [25]. This was specifically selected to show that the prediction methods presented are applicable to larger cabinet sizes and beyond the vertical domain. For mechanical reasons a small array of 3 SEQUENZA 10N boxes was used. The front height of a cabinet is about 0.30 m, the overall size of the stacked array is approximately 0.91 m.

[3]We might also imagine that, as part of the end-of-line test, these data could be programmed into an intelligent active loudspeaker. Optimization software could then recover this information via the network to improve the accuracy of the result.

The array was modeled by a GLL and its performance simulated with EASE SpeakerLab. In this model each cabinet contains three different complex directivity point sources, one each for the LF, LF/MF, and HF transducer. The controller settings for the crossover and EQ were measured separately and also applied in the GLL.

All of the balloon measurements were made at a distance of 8 m so that the far-field condition is still fulfilled. Full-sphere complex data were acquired. For the single box all three transducer measurements were performed about the same point of rotation, namely, the geometric center of the cabinet. In this respect we remark that the use of phase data in the prediction automatically accounts for the spatial offset of the transducers relative to the point of rotation [14]. Also the single box measurements were made without either top or bottom neighbor, which is equivalent to the isolated case, as defined before. The HF driver was measured with 2° resolution, the LF and LF/MF drivers with 5°.

For the array measurements the system was rotated about the geometric center of the center box. The backside of the array was not measured. The angular resolution of the array measurement along a meridian was 2°, and the horizontal resolution along a parallel was 30°.

3.2.2 Polar Response

Because we have already presented a detailed investigation of the CDPS model in the vertical domain, our intention here is mainly to show that the concept works

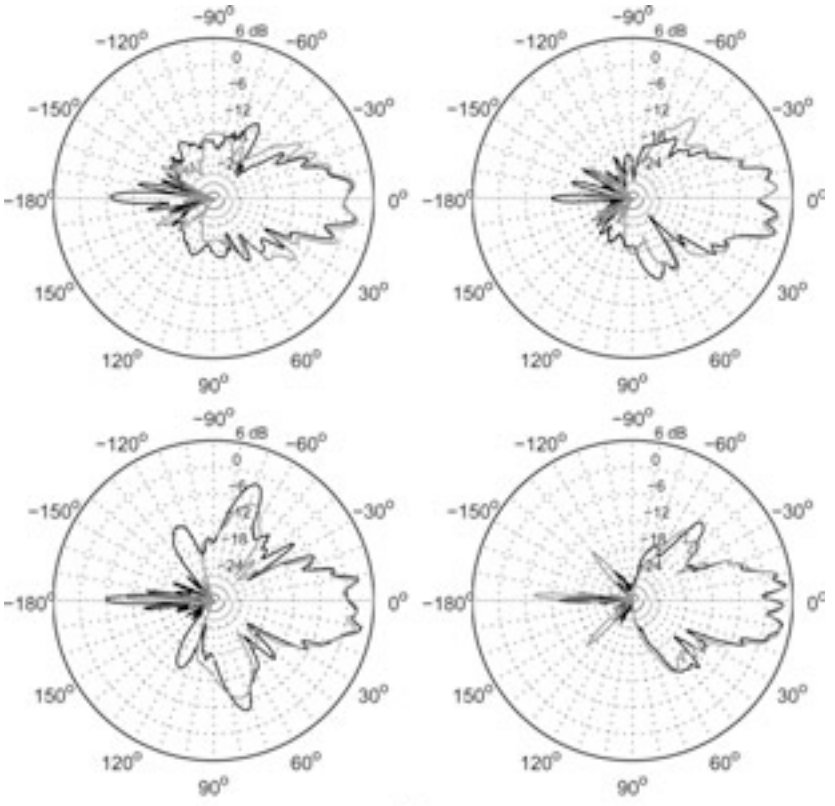

Fig. 18. *Continued*

similarly well for any other domain. For this purpose we have chosen a set of cross-sectional polar plots at the crossover frequency of the system. The array presented here uses splay angles of 0° between adjacent elements (Fig. 19). Other frequencies and configurations have been examined as well but do not provide additional insights.

Fig. 20(a) and (b) show the horizontal and vertical polar plots at 1250 Hz smoothed to a bandwidth of one-sixth octave for better comparison. The radial scale is 40 dB, and 0° denotes the on-axis direction, 90° the upward direction.

Diagonal polar plots are presented in Fig. 20(c)–(f). Four different diagonal planes are shown, namely, 30°/210°, 60°/240°, 120°/300°, and 150°/330° rotated about the system axis in clockwise direction, where the left is 0° when looking out of the box.

Obviously the correlation between measured and predicted performances is very good. Within an opening angle of about 50° the deviations are typically within ±2 dB. Because the measurements were made for an isolated cabinet, some of the improvements introduced earlier and affecting off-axis prediction accuracy do not apply here. Therefore the deviations in the polar responses increase to about ±3 dB for larger angles.

Overall we can state that the simulation matches the measurement very well, and this includes planes other than horizontal and vertical.

4 COMPARISON WITH ALTERNATIVE METHODS

After having presented a detailed investigation of the CDPS model in the previous section we want to compare it briefly with other known approaches that are utilized to model the radiation characteristics of continuous sound sources.

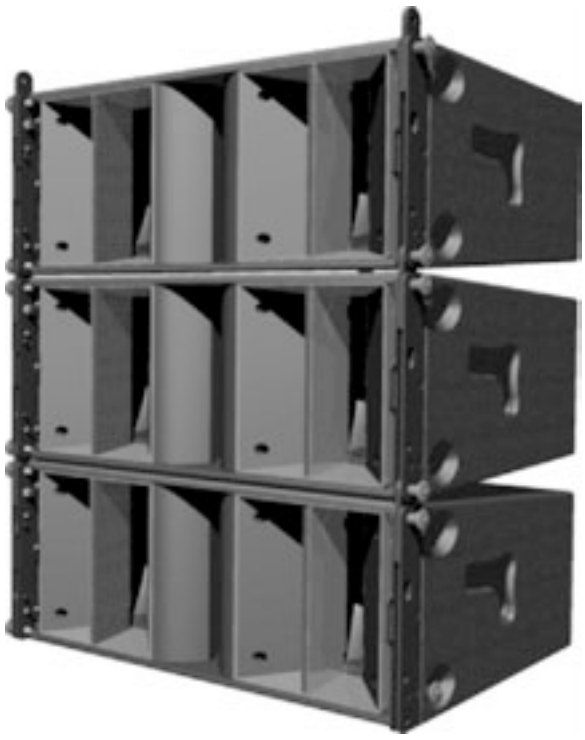

Fig. 19. Straight array of three SEQUENZA 10N cabinets as modeled in EASE SpeakerLab.

4.1 Elementary Sources Method

The Huygens principle [1] states that a propagating wavefront can be reproduced by a set of discrete point sources located on that wavefront [Eq. (7)]. Various attempts have been made to employ Huygens' principle as a computational radiation model for curved or linear sound sources; see, for example, [2], [3].

In its simplest form this concept is only applied in the vertical domain. The radiation from the mouth of a horn or waveguide is measured at a specific distance and then modeled by a linear array of omnidirectional point sources, which are located close to each other compared to the wavelength and which represent a line of constant phase. More advanced versions allow curved or arbitrarily shaped vertical arrays of directional sources. Beyond the purely vertical domain this Huygens model can be extended to the horizontal domain as well by utilizing two-dimensional arrays of sources to represent two-dimensional sound-radiating surfaces.

All of these approaches need to be combined with an extensive set of actual measurement data. The more degrees of freedom are available regarding source count, directionality, and placement the more measurements are needed to find optimal reproduction parameters. Due to the complexity of the optimization process and its convergence for the more advanced models, the calibration of such a source array can be a tedious procedure.

It is an advantage of this approach that no phase data have to be acquired directly, especially compared to the CDPS model. It is also sometimes beneficial that a well-defined Huygens model is able to reproduce the near field of the radiating source where the CDPS model relies on far-field elemental data.

On the other hand, the computational efforts for the directivity prediction are much higher. Considering a resolution requirement of a half-wavelength, a vertical model of a 0.3 m line source has to include at least 18 sources to be valid up to 10 kHz. Compared to the CDPS model of the cabinet, possibly using just a single source, necessary calculation times are higher by an order of magnitude. Extensions to the horizontal domain further increase the computational demands.

Another disadvantage of the Huygens approach is its lack of generality regarding off-axis radiation angles. Naturally the wavefront principle cannot be applied when planes of constant phase are difficult to measure or do not exist. This is true especially for the sides and the backside of a typical loudspeaker cabinet. In addition to that, wavefront models that consist of only a vertical array of sources need to approximate the pressure radiation for the horizontal domain. This is often accomplished by including a conventional directivity measurement of the horizontal plane. However, it is questionable and remains to be proven that for the diagonal planes there exist interpolation methods of satisfying accuracy.

4.2 Integral Methods

An extremely accurate solution to the problem of determining the acoustic field exterior to an object with

radiating elements exists in the form of the boundary-element method (BEM) [23]. Here a numerical approximation to the Helmholtz wave equation is determined, which incorporates practically all of the acoustic phenomena. Unfortunately an application of the method to a complete array over the entire audible frequency range presents a formidable computational obstacle. Largely for this reason researchers have concentrated on applying the methods to individual radiating components within a single array element.

In an effort to reduce the scale of the problem some attempts have been made to apply Rayleigh integral techniques [4] to characterize a radiating component within an array. The complex pressure or normal velocity is deduced over a small flat surface in front of the component. Once known, the exterior field can be determined in front of the plane. The idea is then to tessellate these surfaces to simulate an array. Leaving aside the inability of the approach to model the rearward radiation there remains the problem of acquiring the surface data. One method is to make some polar measurements of the device and use them as a target in an optimization loop that attempts to determine the surface data [5]. Direct measurement of the data may also be possible [6]. Alternatively, for horns one could view the problem as an interior BEM solution, with appropriate boundary conditions on the imagined surface, thus obtaining surface data based on the real horn geometry [26].

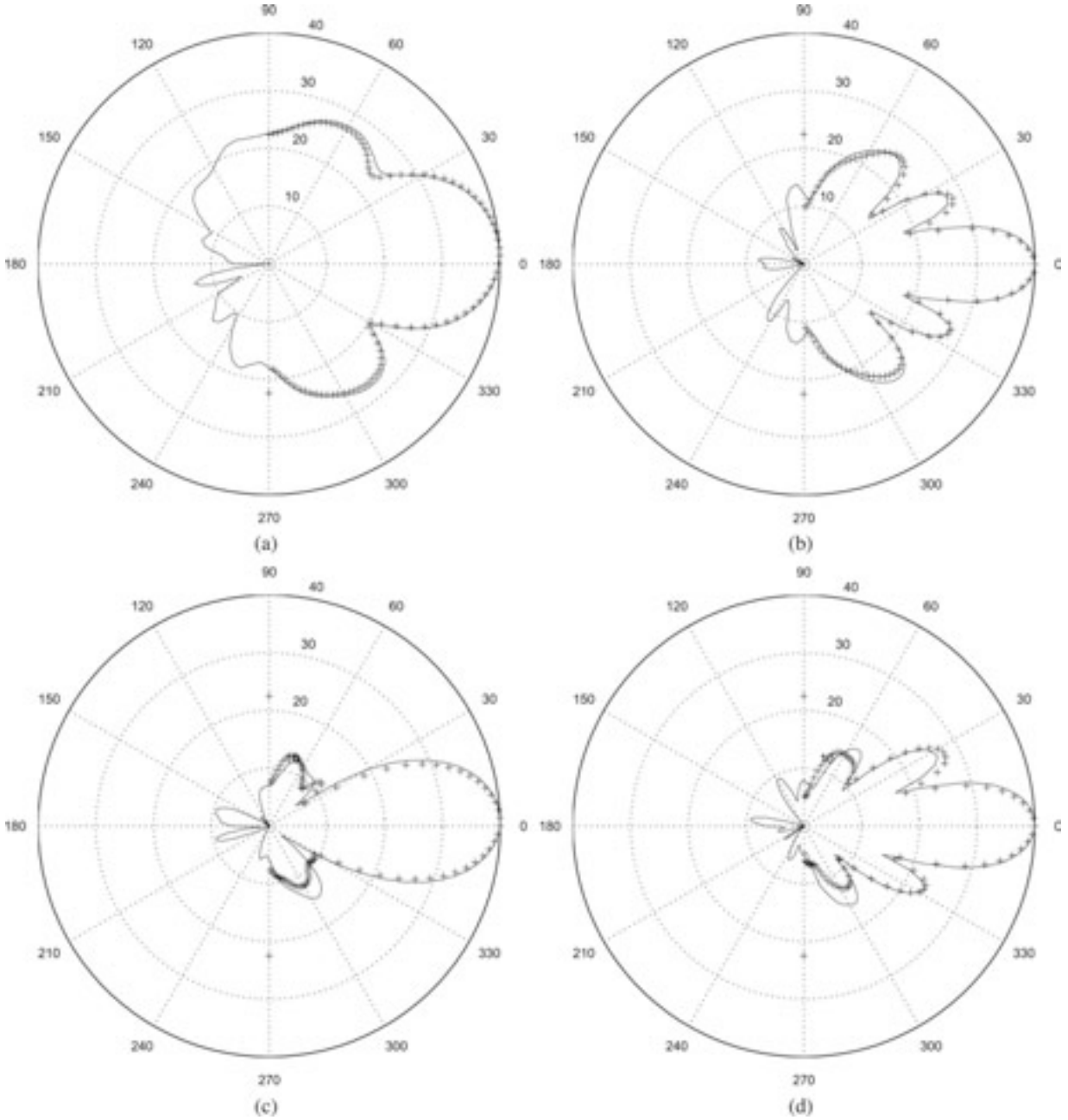

Fig. 20. Polar plots of array at 1250 Hz; measured data (+++) and predicted data (—). (a) Horizontal. (b) Vertical. (c) Diagonal (30°/210°). (d) Diagonal (60°/240°). (e) Diagonal (120°/300°). (f) Diagonal (150°/330°).

Assuming accurate surface data for one component are available, there still remains the problem of the influence of the rest of the array. To illustrate this, a midfrequency horn in a medium-sized touring line array has been modeled using BEM. Fig. 21(a) shows the 400-Hz pressure magnitude on an imagined surface just behind the grille. The surface extends over a six-box array with the active box at second position from the top. Fig. 21(b) shows the effect of simply

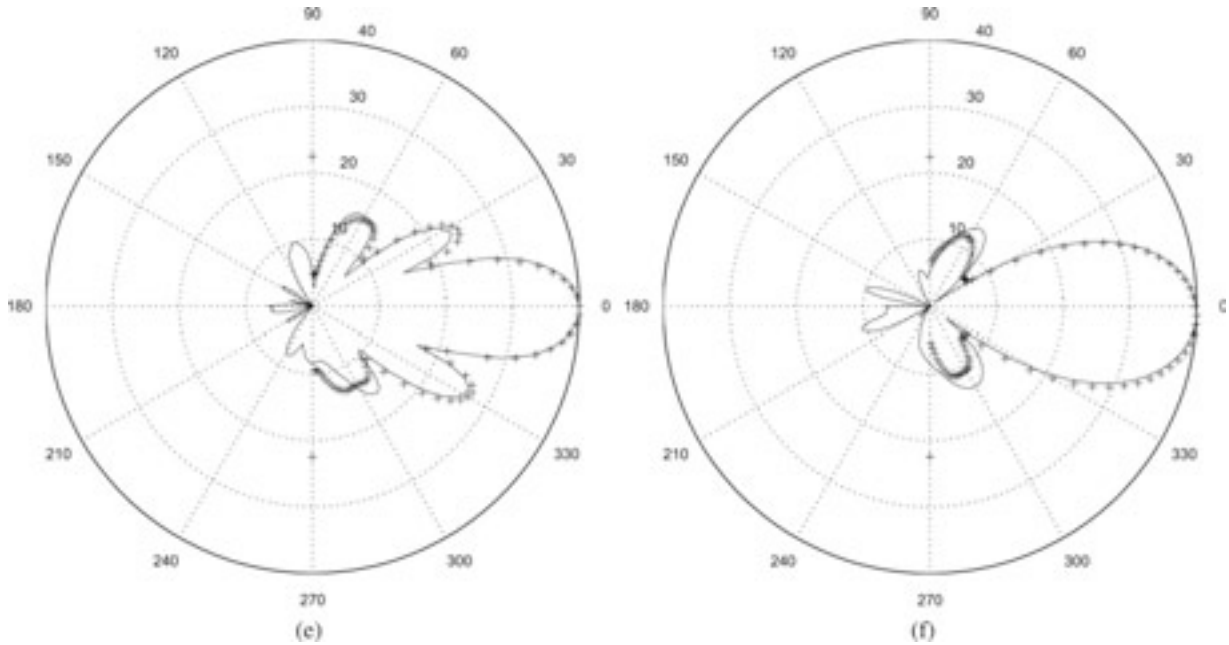

Fig. 20. *Continued*

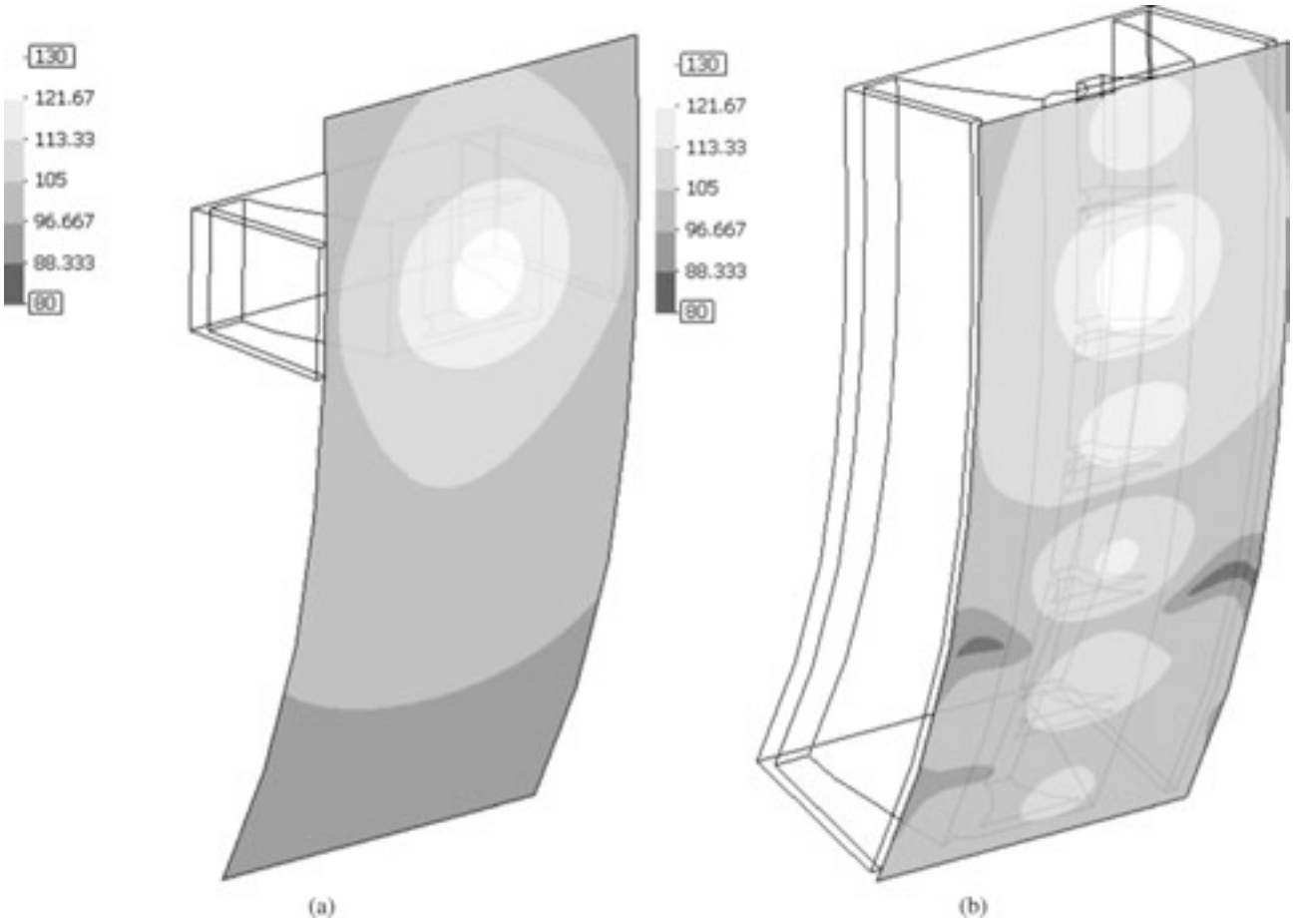

Fig. 21. Modeled pressure magnitude at 400-Hz frequency. (a) Imagined surface in front of isolated loudspeaker. (b) Imagined surface in front of an array of six loudspeakers with only the second box being active.

placing inactive elements above and below the active one. Obviously one will obtain quite different results for the exterior fields for these two configurations at this frequency.

The integral approaches can be useful for designing components or modeling isolated loudspeakers. However, when applied to wide-band array predictions they have similar limitations as the isolated case of the CDPS. Many of the concerns these methods address, such as geometric error mechanisms, are solved by the use of complex data in the CDPS model. So it seems that the considerable measurement or analysis burden to create such models is not warranted. Full BEM of the entire array at low and mid frequencies is feasible. A combination of a CDPS model operating in the region of geometrical acoustics [27] and BEM operating below that frequency would seem almost ideal.

5 CONCLUSIONS

With this work we have introduced a refined computational model based on complex-directivity point sources to predict the performance of extended loudspeaker arrays in a simple, consistent, and closed form. Although the use of phase data and directional point sources for prediction purposes in itself is not new, for the first time we show its broad applicability, quantify its accuracy, and present implementations based on several platforms.

We first introduced the CDPS model as a simple means to simulate loudspeakers and loudspeaker arrays. Based on that, we have shown that the sound radiation characteristics of any continuous line source can be reproduced by this model within given error limits. We have also derived principal conditions for the description by discretized complex directivity data.

Subsequently we made detailed comparisons between measured and predicted results for two different arrays. It was shown that taking into account the effect of neighboring cabinets on the radiation behavior of a particular line array element can significantly improve the overall prediction accuracy, particularly the absolute sensitivity. We have also seen that production variations of elements of the line array which are assumed to be identical have a limited but noticeable effect on the error of the simulation results. Finally we showed that the CDPS model is generally valid in three dimensions without restriction.

We concluded with some remarks about alternative approaches in the last section of this work. There exist several other computational models for the sound radiation of a loudspeaker of accuracy comparable to the CDPS model. However, they are typically more difficult to implement, computationally expensive, and limited in their general applicability.

With direct realizations in EASE SpeakerLab based on the GLL framework, in DISPLAY v1.6 and v2.0, as well as in MATLAB we have demonstrated the technical simplicity and accuracy of the CDPS model. Complemented by measurements of sufficient accuracy or a precise BEM- or FEM-based model for the cabinet itself this approach provides a high degree of confidence for the prediction of sound radiation by a loudspeaker array.

Accordingly, the authors would like to emphasize that given the performance and memory of modern PC platforms there should no longer be any major issues hindering the implementation and utilization of an accurate prediction model for complex loudspeaker systems based on fairly simple input data.

6 ACKNOWLEDGMENT

The authors would like to thank their teams at Ahnert Feistel Media Group and at Martin Audio for their continued support and efforts during the extensive research work. They are grateful for many spirited discussions with Jason Baird, Rainer Feistel, Stephen Kirkup, and Anselm Goertz. They are also thankful to José Ramón Menzinger and Martin Kling from Kling & Freitag for the provision of measurement data and in-depth support.

7 REFERENCES

[1] B. B. Baker and E. T. Copson, *The Mathematical Theory of Huygens' Principle*, 2nd ed. (Oxford University Press, London, 1953).

[2] A. Gloukhov, "A Method of Loudspeaker Directivity Prediction Based on Huygens–Fresnel Principle" presented at the 115th Convention of the Audio Engineering Society, *J. Audio Eng. Soc. (Abstracts)*, vol. 51, p. 1256 (2003 Dec.), convention paper 5985.

[3] V. Holtmeyer, "Line Array Loudspeaker System Simulation with the Ulysses CAAD Software," Diploma thesis, http://www.ifbsoft.de/publication/documents/e_Diploma%20Thesis_VH_Simulation%20Of%20Line-Arrays.pdf (2002 Oct.).

[4] E. G. Williams, *Fourier Acoustics*, 1st ed. (Academic Press, London, 1999).

[5] D. W. Gunness and W. R. Hoy, "Improved Loudspeaker Array Modeling—Part 2," presented at the 109th Convention of the Audio Engineering Society, *J. Audio Eng. Soc. (Abstracts)*, vol. 48, p. 1104 (2000 Nov.), preprint 5211.

[6] M. Di Cola and D. Doldi, "Horn's Directivity Related to the Pressure Distribution at Their Mouth," presented at the 109th Convention of the Audio Engineering Society, *J. Audio Eng. Soc. (Abstracts)*, vol. 48, p. 1104 (2000 Nov.), preprint 5214.

[7] S. Feistel and W. Ahnert, "Modeling of Loudspeaker Systems Using High-Resolution Data," *J. Audio Eng. Soc.*, vol. 55, pp. 571–597 (2007 July/Aug.).

[8] Martin Audio, DISPLAY 1.6 software, http://www.martin-audio.com.

[9] H. Staffeldt and A. Thompson, "Line Array Performance at Mid and High Frequencies," presented at the 117th Convention of the Audio Engineering Society, *J. Audio Eng. Soc. (Abstracts)*, vol. 53, p. 109 (2005 Jan./Feb.), convention paper 6274.

[10] MATLAB software, http://www.matlab.com.

[11] EASE SpeakerLab software, http://www.afmg.eu.

[12] Martin Audio, DISPLAY 2.0 software, http://www.martin-audio.com.

[13] L. Kinsler, A. Frey, A. Coppens, and J. Sanders, *Fundamentals of Acoustics*, 4th ed. (Wiley, New York, 2000).

[14] S. Feistel and W. Ahnert, "The Significance of Phase Data for the Acoustic Prediction of Combinations of Sound Sources," presented at the 119th Convention of the Audio Engineering Society, *J. Audio Eng. Soc. (Abstracts),* vol. 53, p. 1240 (2005 Dec.), convention paper 6632.

[15] W. Ahnert, S. Feistel, J. Baird, and P. Meyer, "Accurate Electroacoustic Prediction Utilizing the Complex Frequency Response of Far-Field Polar Measurements," presented at the 108th Convention of the Audio Engineering Society, *J. Audio Eng. Soc. (Abstracts)*, vol. 48, p. 357 (2000 Apr.), preprint 5129.

[16] S. Feistel, W. Ahnert, and S. Bock, "New Data Format to Describe Complex Sound Sources," presented at the 119th Convention of the Audio Engineering Society, *J. Audio Eng. Soc. (Abstracts)*, vol. 53, pp. 1239, 1240 (2005 Dec.), convention paper 6631; GLL format specification, http://www.afmg.eu.

[17] H. Staffeldt, "Prediction of Sound Pressure Fields of Loudspeaker Arrays from Loudspeaker Polar Data with Limited Angular and Frequency Resolution," presented at the 108th Convention of the Audio Engineering Society, *J. Audio Eng. Soc. (Abstracts)*, vol. 48, p. 357 (2000 Apr.), preprint 5130.

[18] F. Seidel and H. Staffeldt, "Frequency and Angular Resolution for Measuring, Presenting, and Predicting Loudspeaker Polar Data," presented at the 100th Convention of the Audio Engineering Society, *J. Audio Eng. Soc. (Abstracts)*, vol. 44, p. 641 (1996 July/Aug.), preprint 4209.

[19] D. Gunness, "Loudspeaker Directional Response Measurement," presented at the 89th Convention of the Audio Engineering Society, *J. Audio Eng. Soc. (Abstracts)*, vol. 38, p. 874 (1990 Nov.), preprint 2987.

[20] S. Feistel, W. Ahnert, C. Hughes, and B. Olson, "Simulating the Directivity Behavior of Loudspeakers with Crossover Filters," presented at the 123rd Convention of the Audio Engineering Society, New York, 2007 Oct. 5–8, convention paper 7254.

[21] EASE software, http://www.afmg.eu.

[22] Martin Audio, Omniline, www.omniline-ma.com.

[23] S. M. Kirkup, *The Boundary Element Method in Acoustics*, 2nd ed., www.boundary-element-method.com.

[24] A. Thompson, "Automated Splay Angle Calculation for Line Array Loudspeaker Systems," presented at Reproduced Sound 22 (2006 Nov.).

[25] Kling & Freitag, SEQUENZA 10N, http://www.kling-freitag.de.

[26] S. M. Kirkup and A. Thompson, "Simulation of the Acoustic Field Produced by Cavities Using the Boundary Element–Rayleigh Integral Method and Its Application to a Horn Loudspeaker," presented at the International Congress on Sound and Vibration (2004).

[27] P. M. Morse, and K. U. Ingard, *Theoretical Acoustics*, 1st ed.; with errata page (Princeton University Press, Princeton, NJ, 1986).

THE AUTHORS

S. Feistel

A. Thompson

W. Ahnert

Stefan Feistel studied physics at the University of Rostock, Germany, and at the Humboldt University, Berlin, Germany, and he received a Master's degree in theoretical physics in 2004.

In 2000, together with Wolfgang Ahnert, he founded SDA Software Design Ahnert GmbH, Berlin, Germany, which is dedicated to the development of acoustic modeling and measuring software. In 2002 the nonprofit organization ADA Foundation was established to support universities and colleges with software products, such as the simulation software EASE and the measurement tool EASERA. To coordinate these activities, the Ahnert Feistel Media Group (AFMG), Berlin, Germany, was established in 2006.

Mr. Feistel has authored or coauthored more than 40 papers on software projects and related mathematical, numerical, and experimental background studies. He is a coauthor of the *Handbook for Sound Engineers*, 4th ed., edited by G. Ballou, and of the *Messtechnik der Akustik*, edited by M. Möser. He is a member of the AES.

●

Ambrose Thompson received an engineering degree in electroacoustics from the University of Salford, UK, in 1996.

He worked as an acoustic engineer in the high-fidelity industry, where he designed a number of loudspeaker systems and drive units. In 2001 he joined Martin Audio Ltd., High Wycombe, UK, as a loudspeaker design engineer and developed interests in the application of the BEM to horn design and loudspeaker system simulation. His most recent published work concerns the use of numerical optimization for loudspeaker component and system design.

●

Wolfgang Ahnert graduated in Dresden, Germany, in 1975.

From 1975 to 1990 he worked in an engineering office in Berlin, Germany. In 1990 he founded ADA Acoustic Design Ahnert, Berlin, Germany. In 2000 he founded SDA Software Design Ahnert GmbH, Berlin, Germany, to increase the output in writing source codes for acoustic and electronic applications. In 2002 the ADA Foundation was established to support universities and colleges with acoustic software, such as EASE and the measurement tools EASERA and EASERA SysTune. To coordinate all these activities, the Ahnert Feistel Media Group, Berlin, Germany, was established in 2006.

He became an honorary professor at the Hochschule für Film- und Fernsehen Potsdam, Germany, in 1993 and at the Lomonossov University Moscow, Russia, in 2001. Since 2005 he has been a visiting professor at the Rensselaer Institute for Architecture, Troy, NY.

Dr. Ahnert is one of the authors of the book *Fundamentals of Sound Reinforcement* (1981, 1984 in Russian) and the book *Sound Reinforcement—Basics and Practice* (1993, 2000 fully updated in English, 2002 in Chinese, and 2003 in Russian). He wrote with coauthors chapters in the *Handbook for Sound Engineers* (3rd edition), the *Handbuch der Audiotechnik* (2008, Springer, in German), and the *Akustische Messtechnik* (2009, Springer, in German). He has also published more than 65 scientific lectures. He is a fellow of the Audio Engineering Society and the Acoustical Society of America, and a member of the German DEGA and the British Institute of Acoustics.